Akbari Zahra (Orcid ID: 0000-0002-5607-5429)
Montazerozohori M. (Orcid ID: 0000-0001-8897-4683)
Hoseini S. Jafar (Orcid ID: 0000-0003-2703-5441)
Naghiha Reza (Orcid ID: 0000-0003-0253-2003)
Hayati Payam (Orcid ID: 0000-0002-9312-3143)
Bruno Giuseppe (Orcid ID: 0000-0001-9791-6653)
Santoro Antonio (Orcid ID: 0000-0002-4015-0359)
White Jonathan (Orcid ID: 0000-0002-0707-6257)

Synthesis, crystal structure, Hirshfeld surface analyses, antimicrobial activity, thermal behavior of some novel nanostructure hexa-coordinated Cd(II) complexes: precursors for CdO nanostructure

Z. Akbari[1,5](Phd student), M. Montazerozohori(PhD)[1*], S. J. Hoseini(PhD)[2], R. Naghiha(PhD)[3], P. Hayati(PhD)[4], G. Bruno(PhD)[5], A. Santoro(PhD)[5], J.M. White(PhD)[6]

[1]Department of Chemistry, Yasouj University, Yasouj 7591874831 Iran.

[2]Department of Chemistry, College of Sciences, Shiraz University, Shiraz, Iran

[3]Department of Animal Sciences, Faculty of Agriculture, Yasouj University, Yasouj, Iran.

[4]Persian Golf Science and Technology Park, Nano Gostran Navabegh Fardayedashtestan Company, Borazjan.

[5]Department of Chemical, Biological, Pharmaceutical and Environmental Sciences, University of Messina, Viale F. Stagno d'Alcontres 31, 98166, Messina, Italy.

[6]School of Chemistry and BIO-21 Institute, 30 Flemington Road, University of Melbourne, Parkville, Australia.

Runing head: Synthesis, structure and some properties of cadmium complexes

***Corresponding author:** mmzohori@yu.ac.ir; mmzohory@yahoo.com; Telfax:+987431001400

Contact author: Zakbari@unime.it; sanazakbari1399@gmail.com; Telfax:+987431001400

This is the author manuscript accepted for publication and has undergone full peer review but has not been through the copyediting, typesetting, pagination and proofreading process, which may lead to differences between this version and the Version of Record. Please cite this article as doi: 10.1002/aoc.6181

Abstract

A new tetradentate Schiff base ligand entitled as (L= (N^2E, $N^{2'}$E)-N^1, $N^{1'}$-(ethane-1,2-diyl)bis(N2-((E)-3-(2-nitrophenyl)allylidene)ethane-1,2-diamine) and its six cadmium(II) complexes formulated as $CdLX_2$ in which X is Cl, Br, I, NO_3,NCS and N_3 were synthesized under ultrasound irradiation and characterized by various physical and spectral techniques. Moreover some complexes were also prepared in nanostructured dimensions confirmed by SEM, EDAX and XRPD techniques and then were used as precursor for preparation of CdO nanoparticles via direct calcination at 600 ˚C. As typical, the crystal structure of cadmium(II) nitrate complex was determined using single crystal X-ray diffraction. Accordingly it was found that $[Cd(L)(NO_3)_2]$ complex crystallizes in the monoclinic space group $P2_1/n$ with two independent molecules in the asymmetric unit with two coordination mode of nitrate anions. This complex has zero-dimensional (0D) coordination supra-molecular structure. Hirshfeld surface analyses suggested that H...O(49.5 %), H...H(30.3 %) and H…C(11.8 %) intermolecular interactions are most considerable in the crystal packing. Computational study of ligand structure leading to electrostatic potentials of the

solid state geometry and some occupied molecular orbitals (HOMO, HOMO-1, HOMO-2 and HOMO-5) prevailing contribution of nitrogen lone pairs are also reported. Thermal behavior studies of the compounds under nitrogen atmosphere from room to 900 ºC revealed that the ligand is completely decomposed without any residual while the complexes are decomposed via 2-4 thermal steps with trace amount of metallic cadmium as residue. Moreover antibacterial and antifungal screening well showed that the complexes inhibit from the growth of the various bacteria and fungi more efficient than free ligand especially against Gram positive bacteria. DNA cleavage potentials of the compounds may be one of the reasons for their anti-microbial activity.

Keywords: Complex, Crystal structure, Hirshfeld, Cadmium(II), Nanostructure.

1. Introduction

In two past decades, the field of coordination compounds has especially attracted a lot of attention due to their interesting properties leading to applications in bioinorganic chemistry, microbiology [1-4], nano-materials [5], pharmaceutical industry and catalytic [6, 7]. Briefly, these groups of materials consist of metal ion centers surrounded by polydentate ligands. These materials demonstrate various structural topologies including one-, two-, and three-dimensional networks resulting from the structure variety of the ligands[8, 9]. In fact, design and synthesis of new coordination compounds is an issue of particular interest due to their different structural with various applications in various scientific and industrial areas [10-12]. In synthetic point of view,

ultrasound irradiation of the reaction is one of the simplest and most practicable methods for synthesis of a variety of nanostructured compounds with desirable sizes [13-17]. The consequences show that as compared with classic synthetic methods including solvent based reaction, solvo-thermal and hydrothermal methods, sonochemical synthesis is a facile, low cost, and environmentally friendly approach for preparation of nano-sized coordination compounds [18]. Accordingly, many researchers have referred application of ultrasound irradiation in synthetic chemistry because ultrasound waves have been found to accelerate chemical reactions in various systems such as homogeneous and heterogeneous reactions [19]. Triethylenetetraamine alone can be coordinated to metal in many forms. In simplest form, this compound acts as a tetradentate ligand with four aminic nitrogen donors [20, 21]. Schiff base ligands based on triethylenetetraamine can also coordinate to metal ion centers in similar mode of this polydentate amine. Cadmium (II) and other group 12 elements as (d^{10}) metal ions, are specifically suited for formation of coordination compounds. The spherical d^{10} configuration allows a flexible coordination environment so that geometries of these coordination compounds can vary from tetrahedral to dodecahedral with severe distortions or idealized polyhedron. Cadmium complexes are the most common coordination compounds in group 12 of elements. Various applications have been reported for the cadmium complexes especially in photo-inorganic chemistry and biological research areas. Among simple compound of cadmium(II), CdO is of importance. CdO is an n-type semiconductor with a narrow band gap (2.2 eV) and high electrical conductivity. Up until now, it

has been widely studied for optoelectronic applications and other applications such as solar cells, photo transistors, photodiodes and gas sensors [22, 23].

During the past decade, our research group has focused on the structural and biological properties of various Schiff base metal complexes [24-29]. We have recently reported the sonochemical synthesis of the nanostructured coordination compounds [30-32]. In this paper, we present a simple sonication-assisted synthesis of a new series of Cd(II) coordination compounds containing a new tetradendate Schiff base ligand based on triethylenetetraamine and their uses for the preparation of nanostructured cadmium(II) oxide. In addition, crystal structure, computational and Hirshfeld surface analyses and thermal behavior of the complexes are investigated. Moreover antimicrobial activities and DNA cleavage potential of all compounds were studied.

2. Experimental

2.1. Materials and methods

All chemicals used in the synthetic and analytical procedures were purchased from commercial suppliers (Sigma–Aldrich, Merck etc.) and used as received. Melting or decomposition temperatures were measured by the Kruss instrument. The ^{1}H and ^{13}C Nuclear Magnetic Resonance spectra (^{1}HNMR and ^{13}CNMR) of the ligand and its cadmium(II) complex were recorded on a Brucker DPX FT/NMR 400 MHz spectrometer in DMSO-d_6 using TMS as the internal standard. The UV–Visible electronic spectra were recorded in dimethylformamide (DMF) solution using JASCOV570 model spectrophotometer (200–800 nm). The FT/IR spectra of all

compounds were carried out by a JASCO-680 in the range of 4000–400 cm^{-1} as KBr pellets. Molar conductivities of the compounds were determined by a metrohm-712 conductometer with a dip-type conductivity cell made of platinum black in 10^{-3} M of DMF solutions at room temperature. A Perkin-Elmer Pyris model instrument was applied for recording of thermo-grams (TG/DTG/DTA) in the range of 25 ˚C up to 900 ˚C under N_2 atmosphere with a heating rate of 20 ˚C/min. X-ray powder diffraction (XRPD) patterns were obtained by an analytical model X′ Pert Pro focus X-ray diffractometer with Cu-Kα radiation (λ= 1.5418 Å). Scanning electron microscopy (SEM) images were obtained by a Hitachi S-1460 field emission SEM using Ac voltage of 20 kV. Ultrasound irradiation was carried out in an ultrasonic bath Bandelin Super Sonorex RK-100H (frequency of 80 kHz). Diffraction data were collected at 100 ºK on a Rigaku Synergy diffractometer using Mo-Kα radiation (λ= 0.71073 Å). The structure was solved by direct methods and refined by full-matrix least-squares based on F^2 with SHELX-2014 using the WinGX software. Hydrogen atoms attached to carbon were placed in the expected geometric positions and treated in riding models while N-H hydrogens were refined isotropically without restraint. The molecular and packing diagrams were generated using the MERCURY and OLEX software. Density functional theory(DFT) calculations were performed by using the GAUSSIAN 09 program package [33] on i7 processor personal computer. The effect of electron correlation on the molecular geometry was taken into account by using Becke's three-parameter hybrid, and the gradient corrected Lee Yang Parr correlational function (B3LYP) [34] employing the quasi-relativistic effective core potential (RECP), the standard basis sets(SDD) and valence basis sets recommended by Stuttgart group

[35]. B3LYP, CAMB3LYP and several other functions such as HSEH1PBE [36], PBEPBE [37], HCTH [38], TPSSTPSS [39], MPW1PW91[40] and LSDA [41] were used in conjunction with SDD in order to test their ability to reproduce the solid state geometry.

2.3. Synthesis of Schiff base ligand

Schiff base ligand (L) was prepared by a condensation reaction between triethylenetetraamine (1 mmol, 0.146 g dissolved in 5 mL of ethanol) and 2- nitrocinnamaldehyde (2 mmol, 0.354 g in 5 mL ethanol) in a 1:2 M ratio. The reaction was performed in an ultrasonic bath for 1 h at room temperature to complete the reaction. The reaction progress was checked by TLC. Afterward, a brownish solution was obtained. Evaporation of solvent led to a brown precipitate as final product that was recrystallized from ethanol/dichloromethane (1:1) solvent mixture.

2.4. Sonochemical synthesis of nano-structured cadmium(II) complexes

Preparation of nano-structured cadmium(II) halide, thiocyanate, nitrate and azide complexes was carried out by dropwise addition of fresh ethanolic solution of ligand into cadmium(II) salts in ethanol (1 mmol in 10 mL). The reaction mixtures were kept in the ultrasound irradiation for 0.5-1 h at room temperature. The obtained precipitates were filtered, recrystallized from ethanol/dichloromethane (1:1) solvent mixture, dried and placed at 70–100 °C under vacuum and then kept in a desiccator over silica gel. The physical and spectral (FT-IR, UV-Visible) data of the compounds have been collected in tables of 1 and 2. The ^{1}H and ^{13}C NMR data of the ligand and its cadmium(II) complexes based on Scheme 1 are found in tables of 3 and 4.

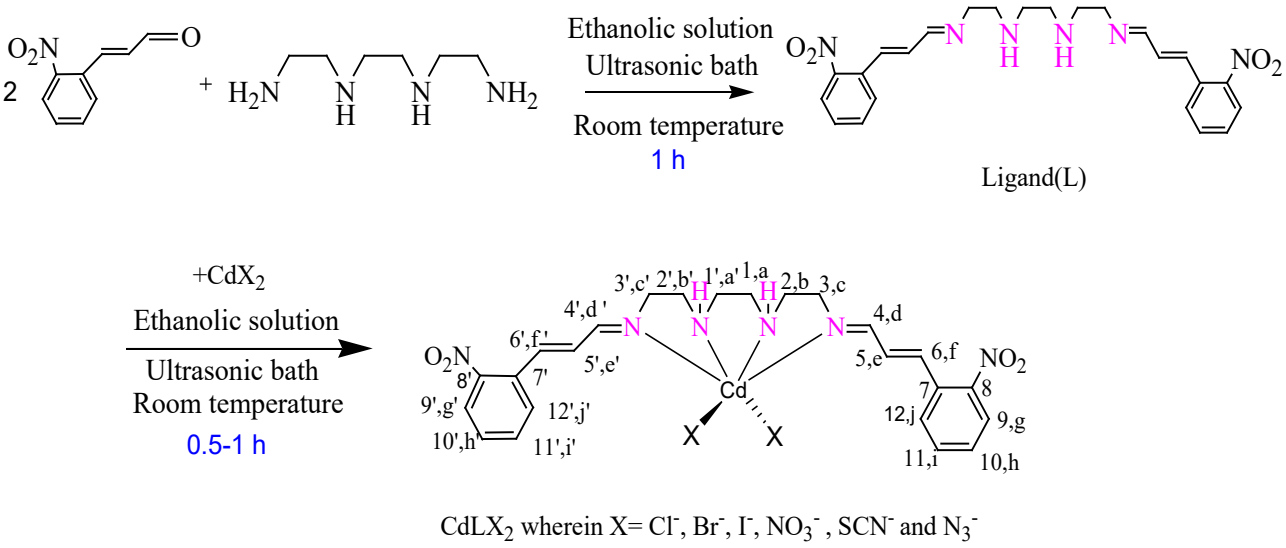

Scheme 1. Synthetic route from ligand to cadmium(II) complexes.

2.5. Preparation of cadmium (II) oxide nanoparticles

For synthesis of CdO nanoparticles, an appropriate quantity of the $CdLI_2$ complex as precursor was transferred into a porcelain crucible and then heated to 600 °C in a furnace under an air atmosphere. After about 4 hour, the resultant powder was washed with a little amount of acetone solvent to discard any impurity and then was dried at 70 ^{O}C for 1 hour to give cadmium(II) oxide nanoparticles.

2.6. *In vitro* antimicrobial activity

The antibacterial activity of the ligand and its cadmium(II) complexes were studied against two Gram-positive bacteria of *Bacillus subtilis* (ATCC: 6633) and *Staphylococcus aureus* (ATCC: 6538); two Gram-negative bacteria of *Pseudomonas aeruginosa* (ATCC: 9027) and *Escherichia coli* (ATCC: 25922) and two fungal species such as *Aspergillus orayzea* and *Candida albicans* in specific concentrations of these compounds (50, 25 and 12.5 mg /mL in DMSO) by the well diffusion method. Based on our previous reports [42], there is no antimicrobial effect for DMSO against the studied microorganisms.

2.7. Minimum inhibitory concentration(MIC) and minimum bactericidal concentration(MBC)

MIC is defined as the lowest concentration of compound which inhibits the growth of microorganism after 24-hour of incubation at 37°C. MICs of the compounds were determined by the serial dilution method. The lowest concentration of the compound that kills the most bacterial population where no dominant growth of the bacteria is observed on the plates is MBC. MBCs data were measured by sub-culturing to Muller Hinton Agar medium on a plate.

2.8. DNA cleavage experiment

DNA cleavage potentials of the ligand and its complexes as compared with H_2O_2 as an oxidant have been studied by agarose gel electrophoresis method. The extraction of DNA was performed according to our previous report[26]. Electrophoresis was run on sample solutions including 4 µL of the solution (prepared by dissolving 5 mg of each compound in 1 mL DMSO) and 4 µL of

extracted DNA. The test samples for the study of DNA cleavage potential were incubated at 37°C for 2 hours. After incubation, the samples were mixed with bromophenol blue dye and along with the standard DNA (alone), the mixture of DNA and H_2O_2 and ladder were loaded carefully into the wells. Electrophoresis was done at constant 100 V of electricity for about 30 minutes. The resulting bands of the electrophoresis were visualized by UV light and then photographed.

3. Results and discussion

3.1. Physical and analytical data

Some physical and analytical data of the titled compounds have been summarized in table 1. The metal complexes are soluble in solvents such as dichloromethane, chloroform, dimethylformamide and dimethylsulfoxide while are insoluble in alcoholic media. All compounds are stable under air atmosphere. The complexation of the tetradentate Schiff base ligand (L) with CdX_2 salts (X= chloride, bromide, iodide, nitrate, thiocynate and azide) in 1:1 M ratio led to the desired complexes with general formula of $CdLX_2$ (Scheme 1) confirmed by elemental analysis as found in table 1. The molar conductivities of the complexes in DMF (10^{-3} M) were obtained in the range of 19.4–23.8 $cm^2\ \Omega^{-1}\ mol^{-1}$ at room temperature confirming their nonelectrolyte nature of them and thus indirectly prove binding of both halide/pseudohalide ions and Schiff base ligand to metal ion center [43-45]. The Schiff base ligand is melted at 147 °C while decomposition temperature of the cadmium(II) complexes is in the range of 183–234 °C.

Table 1. Analytical and physical data of the Schiff base ligand and its Cd(II) complexes.

Compounds	Color	Melting point (dec.)/ ºC	Yield, %	Found(Calculated)/%			$\Lambda_M(\Omega^{-1}\ cm^2\ mol^{-1})$
				C%	N%	H%	
Ligand	Brown	147	70	61.9(62.06)	17.8(18.09)	6.2(6.06)	19.40
$CdLCl_2$	Cream	201	82	44.3(44.50)	13.2(12.97)	3.5(3.36)	22.70
$CdLBr_2$	Yellow	183	85	39.3(39.13)	11.5(11.41)	3.7(3.83)	22.60
$CdLI_2$	Yellow	203	85	34.5(34.70)	10.3(10.12)	3.5(3.40)	22.20
$CdL(NO_3)_2$	Cream	234	68	32.7(32.51)	14.3(14.22)	3.3(3.18)	23.80
$CdL(NCS)_2$	Orange	211	75	34.6(34.38)	16.3(16.40)	3.3(3.15)	22. 80
$CdL(N_3)_2$	Orange	226	71	43.8(43.61)	25.5(25.43)	4.3(4.27)	22.40

3.2. FT/IR spectra

Some selected FT/IR spectral data of the Schiff base ligand and its cadmium(II) complexes have been presented in table 2. The ligand spectrum displays a sharp peak at 1635 cm^{-1} related to azomethine -C═N- bond shifting to higher wavenumbers by 4–6 cm^{-1} in the complexes spectra. The shift of this absorption peak as well as the increase of its intensity in IR spectra of all cadmium(II) complexes confirms the participation of the azomethine group nitrogen in coordination to metal ion center [25-28]. On the other hand, , the absence of characteristic peaks at 1685 and 3289 cm^{-1} related to carbonyl and amine groups stretching vibrations of the starting materials respectively in IR spectrum of ligand may be another evidence for the formation of Schiff base ligand after a condensation reaction [25-27]. The two sharp peaks at 1523 and 1346 cm^{-1} in the ligand spectrum are attributed to the asymmetric and symmetric stretching vibrations of NO_2 groups respectively. In the cadmium(II) complexes spectra, these strong peaks shift a few wavenumbers. Very strong bands at (1569,1307), (2071, 2021) and 2044 cm^{-1} in the IR spectra of the complexes; $CdL(NO_3)_2$, $CdL(NCS)_2$ and $CdL(N_3)_2$ are safely assigned to the coordinated *O*-NO_3, *N*-NCS^- and N_3^- anions respectively [46]. The peaks in the range of 2801 to 3066 cm^{-1} in the

IR spectra of the compounds are assigned to stretching vibrations of iminic, aliphatic and olefinic C—H bonds. Worth mentioning that an other evidence for coordination of the free ligand to metal center is appearance of a weak peak in the region of 400-500 cm^{-1} attributing to stretching vibrations of M-N bonds.

Table 2. IR wavenumbers (cm^{-1}) and electronic data (nm) of the Schiff base (L) and its Cd(II) complexes.

Compound	ν NH amine	ν CH alkene	ν CH aliph.	ν CH imine	ν (SCN/ N_3/NO_3)	ν (C=N)	ν (C=C)	ν (C-N)	ν (NO_2)	ν (M-N)	$\lambda_{(nm)}$ (ε, cm^{-1} M^{-1})
Ligand	3432	3066	2923	2850	-	1635	1459	1160	1523,1346	-	**267(93741), 319 (sh) (33934)**
$CdLCl_2$	3478	3056	2908	2857	-	1639	1430	1164	1519,1338	443	**269(8772),**
$CdLBr_2$	3478	3050	2919	2868	-	1639	1442	1168	1569,1346	408	**268(94584)**
$CdLI_2$	3475	3057	2908	2857	-	1641	1442	1168	1569,1315	447	**269(89397)**
$CdL(NO_3)_2$	3470	3066	2919	2860	1569,1307	1639	1430	1168	1523,1342	447	**268(96327)**
$CdL(NCS)_2$	3470	3023	2919	2865	2071,2021	1639	1465	1168	1569,1346	424	**269(86111),**
$CdL(N_3)_2$	3436	3055	2919	2863	2044	1640	1442	1122	1519,1342	480	**269(58291)**

3.3. Electronic spectra description

The UV–Visible spectra of the ligand and its cadmium(II) complexes were recorded in DMF solution (10^{-5} M) at room temperature. The electronic spectra of the Schiff base ligand and its cadmium(II) complexes are shown in Fig. 1 and the spectral data are given in table 2. The electronic spectrum of the Schiff base ligand exhibits two considerable absorption bands, one at 267 nm (ε= 93741 $cm^{-1}.M^{-1}$) as sharp peak that may be assigned to intra-molecular electronic transitions ($\pi \rightarrow \pi^*$) of olefinic bond and benzene rings [26-28]. In all synthesized complexes spectra, this band has a weak red shift to longer wavelengths by 1-2 nm. The second band at 319 nm (ε= 33934 $M^{-1}.cm^{-1}$) as shoulder is attributed to $\pi \rightarrow \pi^*$ of azomethine groups.

In all complexes, this band is merged to before band. The observed blue shift here is due to coordination to metal ion via the azomethine nitrogen atoms.

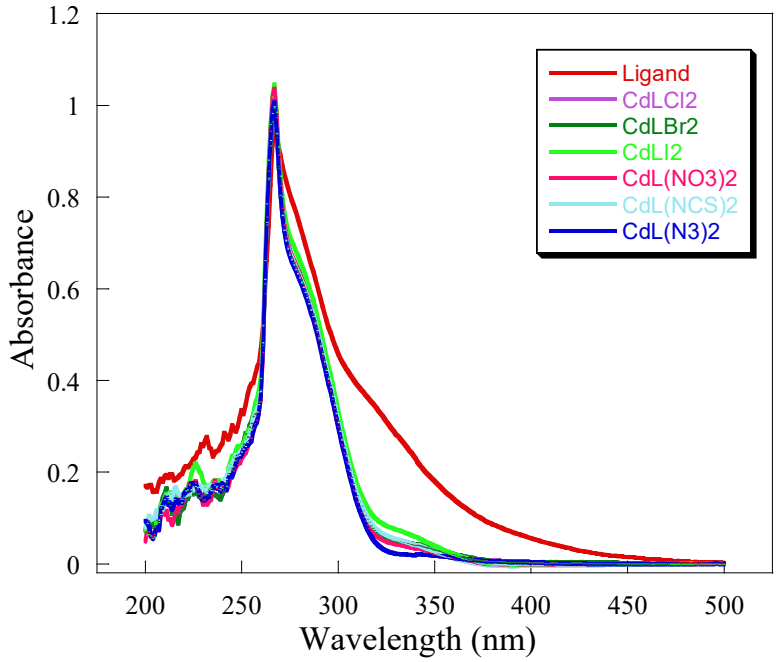

Fig. 1. Electronic spectra of the ligand and its cadmium(II) complexes

3.4. ^{1}H and ^{13}C NMR spectra

In continuation of FT/IR and UV-visible spectral characterization, the ligand and its cadmium(II) complexes were subjected to ^{1}H and ^{13}C NMR spectral study. **^{1}H and ^{13}C NMR** spectra of the ligand and two cadmium(II) complexes as representative are depicted in the fig. 2 and the others are found as fig.1S-11S in supplementary information(SI). The spectral data have been tabulated as tables of 3 and 4. A comparative assignment of the NMR signals of the complexes with respect to the free ligand based on

scheme 1 can well confirm the successful formation of them under current conditions. A characteristic signal of the Schiff base ligand assigned to azomethine protons of dd' appear as a doublet peak at 8.17 ppm. In the complexes **^{1}H NMR** spectra, the signals in the range of 8.42-8.58 ppm can be safely attributed to the azomethine group protons. This is a powerful evidence indicating coordination of azomethine nitrogen atoms of Schiff base to cadmium(II) center.

Table 3. ^{1}HNMR spectral data of the ligand and its cadmium(II) Schiff base complexes in DMSO-d_6

Compound	^{1}H NMR Data (δ, ppm)
Ligand	8.17 (d, $2H_{dd'}$, J= 8.5 Hz), 8.03(d, $2H_{gg'}$, J= 7.8 Hz), 7.96 (t, $2H_{ii'}$, J= 7.8 Hz), 7.76 (t, $2H_{hh'}$, J= 8.0 Hz), 7.63 (d, $2H_{jj'}$, J= 8.0 Hz), 7.36 (d, $2H_{ff'}$, J= 15.5 Hz), 6.95 (dd, $2H_{ee'}$, J_1= 15.3 Hz, J_2= 8.2 Hz), 3.60- 3.57 (m, $4H_{cc'}$), 3.20 (s, $2H_{NH}$), 1.26 (m, $4H_{bb'}$), 0.88 (s, $4H_{aa'}$)
$CdLCl_2$	8.42 (d, $2H_{dd'}$, J= 8.0 Hz), 8.02(d, $2H_{gg'}$, J= 8.0 Hz), 7.82 (d, $2H_{jj'}$, J= 8.0 Hz), 7.67 (t, $2H_{ii'}$, J= 8.0 Hz), 7.60 (t, $2H_{hh'}$, J= 8.0 Hz), 7.54 (dd, $2H_{ee'}$, J_1= 16 Hz, J_2= 8.0 Hz), 7.49 (d, $2H_{ff'}$, J= 16 Hz), 3.73 (s, $4H_{cc'}$), 3.46 (s, $2H_{NH}$), 2.90 (s, $4H_{bb'}$), 2.74 (s, $4H_{aa'}$)
$CdLBr_2$	8.47 (d, $2H_{dd'}$, J= 5.9 Hz), 8.02(d, $2H_{gg'}$, J= 7.7 Hz), 7.79 (d, $2H_{jj'}$, J= 7.3 Hz), 7.67-7.56 (m, $2H_{ii',hh'}$), 7.54 (d, $2H_{ff'}$, J= 14.9 Hz), 7.53 (m, $4H_{ee',ff'}$), 3.73 (s, $4H_{cc'}$), 3.54 (b s, $2H_{NH}$), 2.90 (s, $4H_{bb'}$), 2.75 (s, $4H_{aa'}$)
$CdLI_2$	8.51 (d, $2H_{dd'}$, J= 8.3 Hz), 8.02(d, $2H_{gg'}$, J= 7.5 Hz), 7.78 (d, $2H_{jj'}$, J= 6.7 Hz), 7.61 (t, $4H_{ii',hh'}$, J= 8.0 Hz), 7.56 (d, $2H_{ff'}$, J= 15.5 Hz) 7.44 (dd, $2H_{ee'}$, J_1= 16.00Hz, J_2= 8.0 Hz), 3.74 (s, $2H_{cc'}$), 3.58 (s, $2H_{NH}$), 2.92 (s, $2H_{bb'}$), 2.76 (s, $2H_{aa'}$)
$CdL(NO_3)_2$	8.58 (d, $2H_{dd'}$, J= 9.1 Hz), 7.97(d, $2H_{gg'}$, J= 7.7 Hz), 7.66 (d, $2H_{ff'}$, J= 15.7 Hz), 7.55-7.50 (m, $6H_{ii',jj',hh'}$), 7.00 (dd, $2H_{ee'}$, J_1= 15.5 Hz, J_2= 9.3 Hz), 3.92 (s, $2H_{NH}$), 3.73(s, $4H_{cc'}$), 2.88 (s, $8H_{aa',bb'}$)
$CdL(NCS)_2$	8.53 (d, $2H_{dd'}$, J= 9.2 Hz), 8.02 (d, $2H_{gg'}$, J= 9.8 Hz), 7.80 (d, $2H_{jj'}$, J= 8.1 Hz), 7.63 (d, $2H_{ff'}$, J= 15.8 Hz), 7.58 (t, $2H_{ii',hh'}$, J= 8.0 Hz), 7.22 (dd, $2H_{ee'}$, J_1= 15.6 Hz, J_2= 9.1 Hz), 3.77 (s, $2H_{NH}$), 3.71 (s, $4H_{cc'}$), 2.88 (s, $4H_{bb'}$), 2.72 (s, $4H_{aa'}$)
$CdL(N_3)_2$	8.52 (d, $2H_{dd'}$, J= 8.5 Hz), 8.00 (d, $2H_{gg'}$, J= 7.7 Hz), 7.81- 7.83 (m, $2H_{jj'}$), 7.69 (b s, $2H_{ii'}$), 7.58 (d, $2H_{ff'}$), 7.56 (s, $2H_{hh'}$), 7.23(d d, $2H_{ee'}$, J_1= 15.2 Hz, J_2= 9.0 Hz), 3.75 (s, $2H_{NH}$), 3.69 (s, $4H_{cc'}$), 2.88 (s, $4H_{bb'}$), 2.73 (s, $4H_{aa'}$)

Table 4. ^{13}C NMR spectral data of ligand and its cadmium-Schiff base complexes in DMSO-d_6

Compound	^{13}C NMR Data (δ, ppm)
Ligand	163.15 ($C_{4,4'}$), 148.24 ($C_{8,8'}$), 134.01 ($C_{6,6'}$), 133.01($C_{11,11'}$), 130.66 ($C_{7,7'}$), 130.35 ($C_{10,10'}$), 129.16 ($C_{12,12'}$), 128.89 ($C_{9,9'}$), 125.01 ($C_{5,5'}$), 67.87 ($C_{3,3'}$), 53.13 ($C_{1,1'}$), 50.84 ($C_{2,2'}$)
$CdLCl_2$	166.97 ($C_{4,4'}$), 148.46 ($C_{8,8'}$), 138.91 ($C_{6,6'}$), 134.06 ($C_{11,11'}$), 131.56 ($C_{7,7'}$), 130.93 ($C_{10,10'}$), 130.39 ($C_{12,12'}$), 128.66 ($C_{9,9'}$), 125.18 ($C_{5,5'}$), 57.80 ($C_{3,3'}$), 48.71 ($C_{1,1'}$), 46.76 ($C_{2,2'}$)
$CdLBr_2$	167.24 ($C_{4,4'}$), 148.44 ($C_{8,8'}$), 139.47 ($C_{6,6'}$), 134.05 ($C_{11,11'}$), 131.04 ($C_{7,7'}$), 130.62 ($C_{10,10'}$), 130.31 ($C_{12,12'}$), 128.62 ($C_{9,9'}$), 125.22 ($C_{5,5'}$), 57.72 ($C_{3,3'}$), 48.57 ($C_{1,1'}$), 46.66 ($C_{2,2'}$)
$CdLI_2$	167.30 ($C_{4,4'}$), 148.39 ($C_{8,8'}$), 139.76 ($C_{6,6'}$), 134.05 ($C_{11,11'}$), 131.09 ($C_{7,7'}$), 130.73 ($C_{10,10'}$), 130.31 ($C_{12,12'}$), 128.63 ($C_{9,9'}$), 125.24 ($C_{5,5'}$), 57.73 ($C_{3,3'}$), 48.53 ($C_{1,1'}$), 46.74 ($C_{2,2'}$)
$CdL(NO_3)_2$	168.49 ($C_{4,4'}$), 148.26 ($C_{8,8'}$), 141.71 ($C_{6,6'}$), 134.01 ($C_{11,11'}$), 131.25 ($C_{7,7'}$), 130.19 ($C_{10,10'}$), 130.08 ($C_{12,12'}$), 128.36 ($C_{9,9'}$), 125.24 ($C_{5,5'}$), 57.51 ($C_{3,3'}$), 48.24 ($C_{1,1'}$), 46.63 ($C_{2,2'}$)
$CdL(NCS)_2$	167.86 ($C_{4,4'}$), 148.37 ($C_{8,8'}$), 140.67 ($C_{6,6'}$), 134.19 ($C_{11,11'}$), 133.71 (C_{SCN}), 131.15($C_{7,7'}$), 130.30 ($C_{10,10'}$), 130.06 ($C_{12,12'}$), 128.88 ($C_{9,9'}$), 125,21 ($C_{5,5'}$), 57.60 ($C_{3,3'}$), 48.36 ($C_{1,1'}$), 46.31($C_{2,2'}$)
$CdL(N_3)_2$	167.59 ($C_{4,4'}$), 148.39 ($C_{8,8'}$), 140.24 ($C_{6,6'}$), 134.02 ($C_{11,11'}$), 131.08 ($C_{7,7'}$), 130.59 ($C_{10,10'}$), 130.19 ($C_{12,12'}$), 128.52 ($C_{9,9'}$), 125.19 ($C_{5,5'}$), 57.47 ($C_{3,3'}$), 48.43 ($C_{1,1'}$), 46.38($C_{2,2'}$)

The aromatic signals of the free ligand protons of (gg', jj') and (ii', hh') are found at 8.03, 7.63, 7.96 and 7.76 ppm as doublet and triplet peaks respectively. These signals are smoothly upfielded and/or downfielded after coordination of ligand to metal ion center and appear in the range of 7.97-8.02, 7.50-7.82, 7.50-7.67 and 7.50-7.67 ppm respectively. It may be related to various torsional angles in the complexes leading to various steric and electronic induction effects that effect on the chemical shifts. The olefinic protons of ff' and ee' in the free ligand structure are observed as doublet of doublet and doublet peaks at 7.36 and 6.95 ppm that shift to the downfielded regions of 7.49-7.66 ppm and 7.0-7.54 ppm after coordination of the ligand respectively. Aliphatic hydrogens signals of cc', bb' and aa' are found at 3.60-3.57, 1.26 and 0.88 ppm as multiple or broad singlet signals. These signals are downfielded and appear in the regions of 3.69-3.74 ppm, 2.88-2.92 and 2.72-.2.88 ppm in the cadmium(II) complexes spectra. Finally amine protons(-NH groups) peak appear at 3.2 ppm that notably are downfielded and observed in the region of 3.46-3.92 ppm due to coordination of amine nitrogen atoms of free ligand to cadmium(II) ion. Along with ^{1}H NMR, assignment and comparison of ^{13}C NMR spectral data (as table 4) confirmed synthesis of the ligand and its complexes. The azomethine carbons ($\mathbf{C_{4,4'}}$) peak as a characteristic carbon signal of free ligand appears at 163.15 ppm. This signal shifts to weak fields in the range of 166.97-168.49 ppm in the complexes spectra due to binding of azomethine groups to cadmium (II) ion. Other aromatic, alkenic and aliphatic carbon signals in the complexes spectra with downfielded and/or upfielded

chemical shifts as compared with free ligand as found in table 4 are in agreement with the suggested structure in scheme 1.

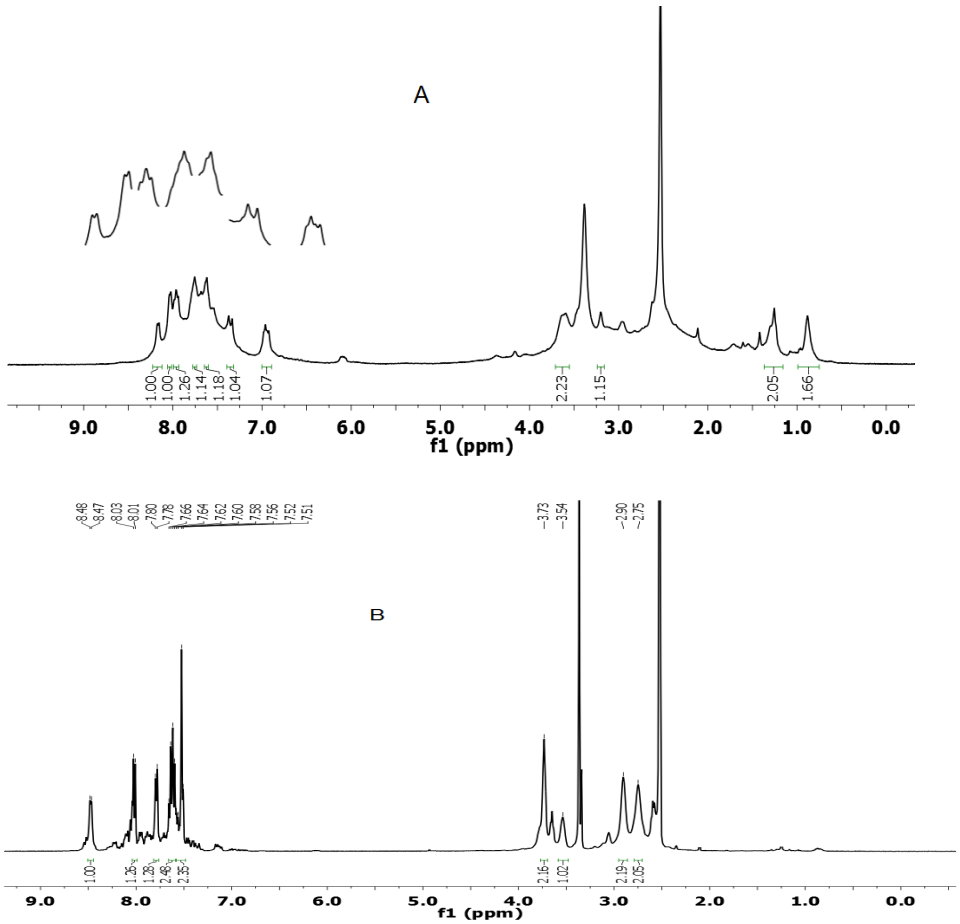

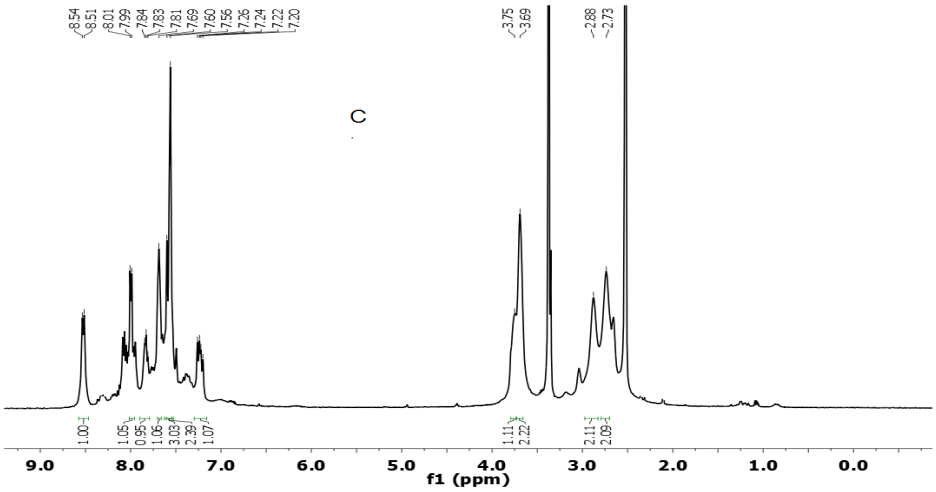

Fig. 2. The ^{1}HNMR spectra of the ligand (A), $CdLBr_2$ (B) and $CdL(N_3)_2$.

3.5. Single crystal structure and computational descriptions of $CdL(NO_3)_2$ complex

Single crystal X-ray diffraction (SCXD) analysis shows that the complex, $CdL(NO_3)_2$ crystallizes in monoclinic system with space group of $P2_1/n$ in an asymmetric unit. $CdL(NO_3)_2$ complex forms zero-dimensional (0D) coordination supra-molecular complex. The asymmetric unit cell of $CdL(NO_3)_2$ includes two different molecules which each one consists of one Cd ion (Cd1 and Cd2), one L, and two coordinated nitrate anions (Fig. 3 and table 5). In $CdL(NO_3)_2$ complex**,** Cd ions are coordinated by eight and six atoms to form distorted octahedral coordination spheres as N_4O_4 and N_4O_2. Each Cd^{+2} cation is coordinated by N atoms of L with Cd(1)-N(2) to N(5) and Cd(2)–N(10) to N(13) distances around 2.33 to 2.45 Å. Nitrate anions coordinate to Cd(II) cation with two types of coordination mode. In Cd (1), two O atoms of each nitrate anion are coordinated by Cd(1)–O(6), O(8), O(9), O(11) distances around 2.35 to 2.68 Å while each nitrate anion is connected via one oxygen atom as Cd (2) with O (18) and O(15) distances around 2.39 Å. (Fig. 4 and table 6).

$CdL(NO_3)_2$ complex is assembled by π_L stacking interactions (centroid– centroid distances of two aromatic rings are 3.770 and 3.727 Å for Cd1 and Cd2 molecules, respectively) (Fig. 5). Generally, it should be noted that the different coordination number, distance and angle of two aromatic rings in $CdL(NO_3)_2$ complex are related to the flexibility of the ligand. The comparison between two aromatic rings reveals that the distance of aromatic rings in Cd2 is nearer than Cd1 leading to change in angle of N-Cd-N in two Cd1 and Cd2 complexes. As shown in fig. 3, angles of N2-Cd1-N5, N10-Cd2-N13 are 142.85° and 139.53°, respectively. There is more space around Cd1, and the anion nitrate is easily connected to Cd1 atoms by two oxygen atoms. Otherwise, Cd2 is more steric hindrance than Cd1 leading to connect one oxygen atom of each nitrate group to Cd2 (table 6).

Hydrogen bonding interactions can be found between O(4), H(54), H(55) and O(10) atoms of ligand as well as nitrite anions respectively (Fig.6 and table 7). Every molecule in crystalline system is also surrounded by another 14 molecules (Fig. 12S in SI).The coordination interactions could be divided into two categories: (a) Fairly strong in the range of 0.826-2.688 Å; (b) Weaker electrostatic in the range of 2.303-3.761 Å. In $CdL(NO_3)_2$ complex, strong bonds assemble monomer complex $CdL(NO_3)_2$ and weak interactions such as hydrogen bond and Van der Waals interactions assemble these complexes leading to a 3D framework with hexagonal like arragement (Fig. 12S in SI). Application of the BFDH (Bravais Friedel Donnay Harker) theory [47] is a simple method for determining the crystallographic types [hkl] most likely to make a crystal habit. It had been carried out in order to approximate the faces growth of the crystal structure solid-state which is occurred along the (10−1) direction (Fig. 7).

Table 5. Crystal data and structure refinement for $CdL(NO_3)_2$ complex.

Empirical formula	$CdL(NO_3)_2$
Formula weight	700.94

Temperature	100.01(10) ºK
Wavelength	1.54184 Å
Crystal system	*Monoclinic*
Space group	$P2_1/n$
Unit cell dimensions	a= 23.5240(4) Å
	b= 8.92200(10) Å
	c= 26.7460(3) Å
Volume	5598.97(13) $Å^3$
Z	8
Density (calculated)	1.663 mg/m^3
Absorption coefficient	6.873 mm^{-1}
F(000)	2848
Crystal size	0.193× 0.153× 0.027 mm^3
Theta range for data collection	2.417 to 77.329°.
Index ranges	-29≤h≤29, -11≤k≤10, -33≤l≤33
Reflections collected	71288
Independent reflections	11718 [R(int) = 0.0552]
Completeness to theta = 67.684°	99.9 %
Absorption correction	Gaussian
Max. and min. transmission	1.000 and 0.331
Refinement method	Full-matrix least-squares on F^2
Data / restraints / parameters	11718/0/791
Goodness-of-fit on F^2	1.062
Final R indices [I>2 sigma(I)]	R_1= 0.0380, wR_2 = 0.1003
R indices (all data)	R_1= 0.0404, wR_2 = 0.1017
R indices (all data)	R_1= 0.0404, wR_2 = 0.1017
Largest diff. peak and hole	1.536 and -1.368 $eÅ^{-3}$

Table 6. Bond lengths [Å] and angles [°] for $CdL(NO_3)_2$ complex.

N(2)-Cd(1)	2.425(3)	N(11)-Cd(2)-N(13)	144.27(10)
N(3)-Cd(1)	2.375(3)	N(11)-Cd(2)-N(12)	75.29(10)
N(4)-Cd(1)	2.352(3)	N(13)-Cd(2)-N(12)	73.72(10)
N(5)-Cd(1)	2.451(3)	N(11)-Cd(2)-N(10)	75.22(10)
N(10)-Cd(2)	2.392(3)	N(2)-Cd(1)-N(5)	142.85(9)
N(11)-Cd(2)	2.333(3)	N(13)-Cd(2)-N(10)	139.59(10)
N(12)-Cd(2)	2.367(3)	N(11)-Cd(2)-O(14)	125.46(9)
N(12)-H(12)	0.82(4)	N(12)-Cd(2)-O(14)	100.55(9)

Table 7. Hydrogen bonds for $CdL(NO_3)_2$ complex[Å and °].

D-H...A	d(D-H)	d(H...A)	d(D...A)	<(DHA)
C(01D)-H(01D)...O(6)#1	0.93	2.40	3.224(4)	147.4
C(8)-H(8)...O(5)	0.93	2.54	3.243(4)	132.8
C(10)-H(10B)...O(11)	0.97	2.55	3.495(4)	164.2
C(11)-H(11A)...O(7)	0.97	2.54	3.241(4)	128.8
C(14)-H(14A)...O(10)	0.97	2.64	3.254(4)	121.7
C(16)-H(16)...O(6)#2	0.93	2.53	3.396(4)	154.2
C(17)-H(17)...O(8)	0.93	2.35	3.063(4)	133.3
C(21)-H(21)...O(15)#3	0.93	2.58	3.474(4)	161.5
C(32)-H(32)...O(14)	0.93	2.55	3.228(4)	130.2
C(34)-H(34A)...O(8)	0.97	2.30	3.271(4)	177.0
C(34)-H(34B)...O(2)	0.97	2.61	3.540(4)	162.0
C(35)-H(35A)...O(15)	0.97	2.50	3.177(4)	127.1
C(38)-H(38A)...O(19)	0.97	2.54	3.244(4)	129.5
C(38)-H(38B)...O(1A)#4	0.97	2.49	3.291(4)	139.8
C(38)-H(38B)...O(12)#5	0.97	2.54	3.064(4)	114.2
C(40)-H(40)...O(1A)#5	0.93	2.45	3.274(5)	147.5
N(12)-H(12)...O(12)#5	0.82(4)	2.50(4)	3.105(4)	132(3)
N(4)-H(4A)...O(3)#2	0.83(4)	2.30(4)	2.999(3)	143(3)
N(3)-H(3A)...O(17)	0.88(5)	2.59(5)	3.419(4)	158(4)
N(3)-H(3A)...O(18)	0.88(5)	2.27(5)	3.059(4)	149(4)
N(11)-H(11)...O(9)	0.90(4)	2.12(4)	2.968(4)	158(4)

Symmetry transformations used to generate equivalent atoms: #1 -x+1,-y+1,-z+1 #2 -x+1/2,y+1/2,-z+3/2 #3-x,-y+1,-z+1 #4 x,y+1,z #5 -x+1/2,y+1/2,-z+1/2

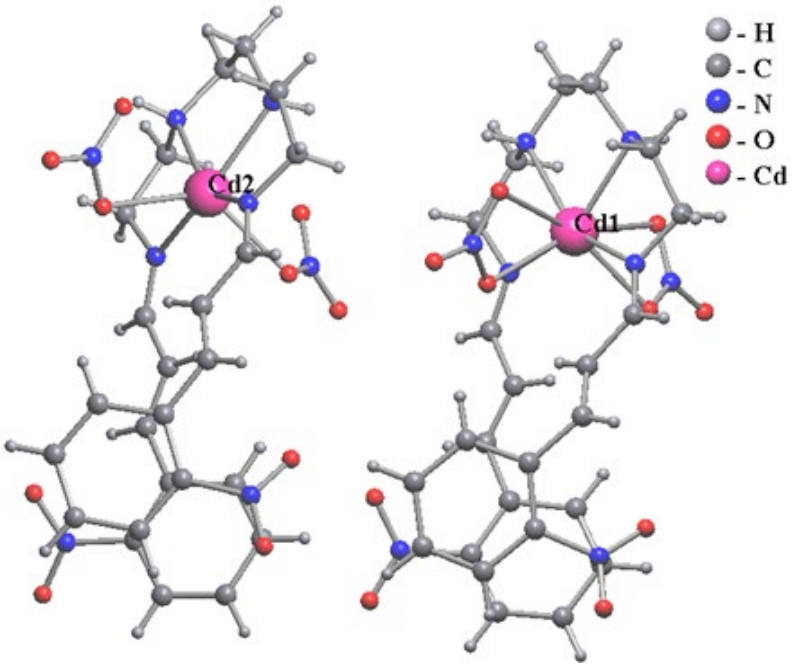

Fig. 3. The coordination environment of Cd atoms in $CdL(NO_3)_2$ complex.

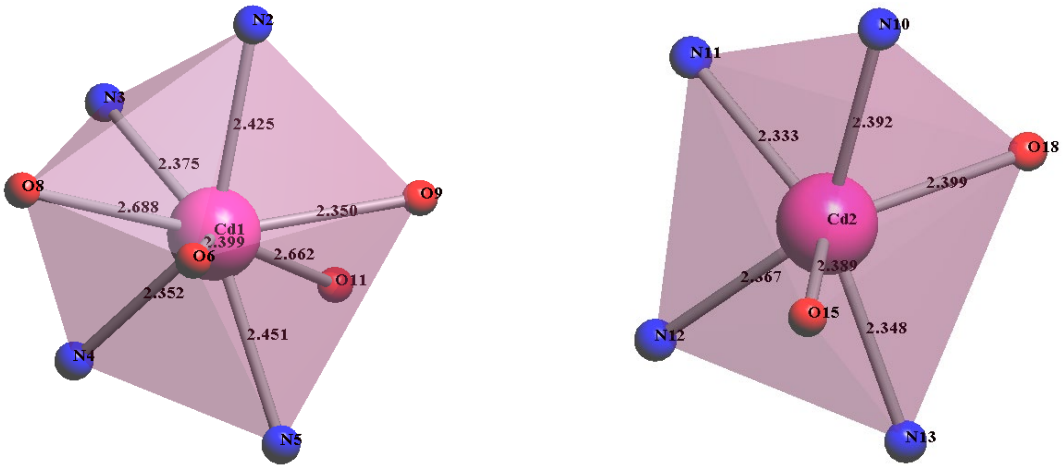

Fig 4. Asymmetric unit cell of $CdL(NO_3)_2$ complex [for Cd1(left) and Cd2 (right)].

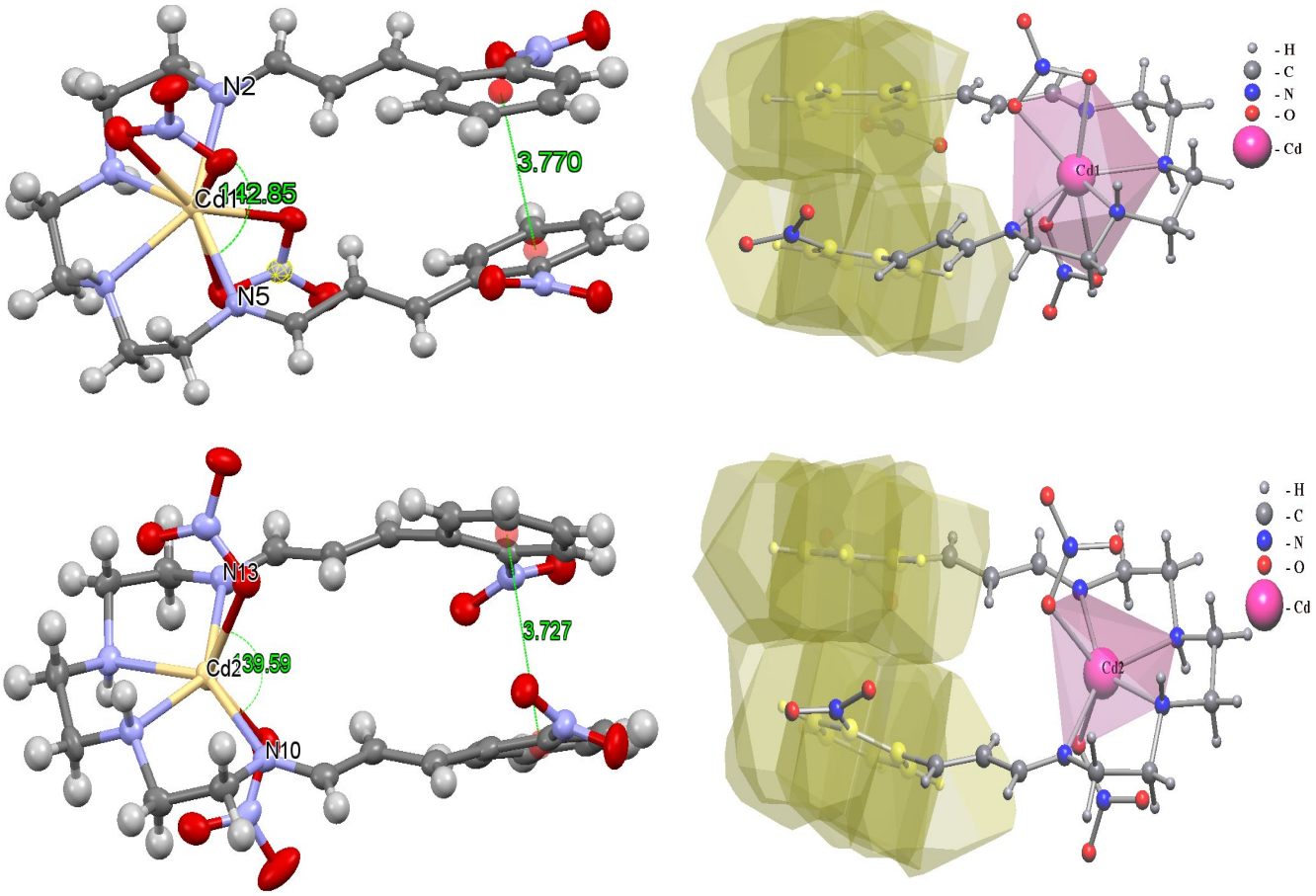

Fig 5. π…π interactions between two aromatic rings of ligand as well as distance of aromatic rings in $CdL(NO_3)_2$ complex.

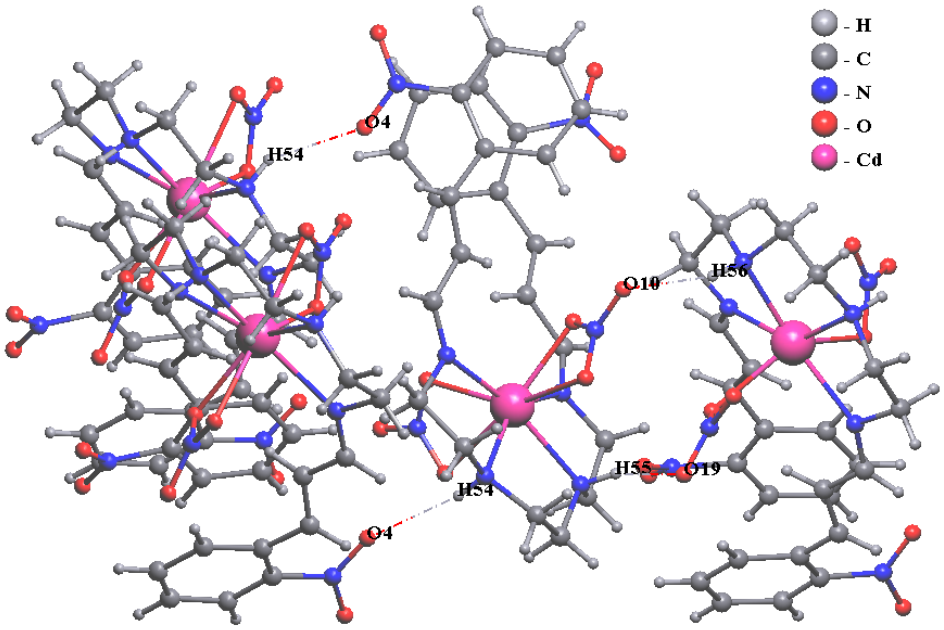

Fig 6. Hydrogen bonds in $CdL(NO_3)_2$ complex.

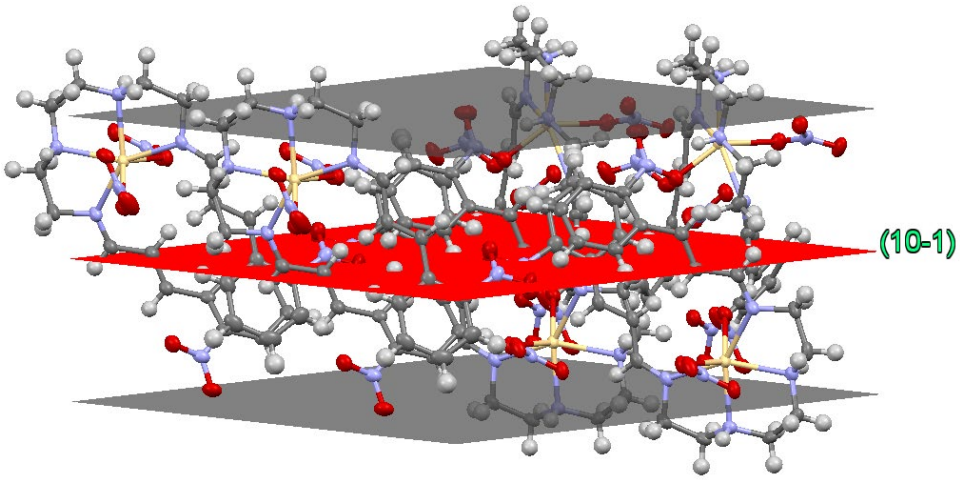

Fig 7. Crystal packing growth along the (10-1) direct for $CdL(NO_3)_2$.

Apart from the crystal structure analysis, a theoretical investigation on the ligand and $CdL(NO_3)_2$ was performed for more clearance of observed results. Accordingly from the structure determined by x-ray, the ligand was subjected to a calculation of single point energy (SPE) at B3LYP/6-311++(2df,2p) level of theory in order to obtain the pictures of its EPS and relevant molecular orbitals. As found in fig.15S(SI), the electrostatic potentials of the solid state geometry and some occupied molecular orbitals (HOMO, HOMO-1, HOMO-2 and HOMO-5) where are prevailing contribution of nitrogen lone pairs, and the LUMO (centred on π* orbital of the phenyl ring) are illustrated. As can be seen in fig.15S(SI), the relevant part of the negative charge is concentrated where it is the site for the coordination to metal atom. In the ligand structure, the separations N..N of imine and N… N amines are 2.863 Å and 4.555 Å respectively. As can be seen from the table SI(supplementary information), the formation of compounds entails a value ≥ 5.2 Å for the N_{imine}-N_{imine} separation.

Similarly to ligand, a series of theoretical calculations were made on the $CdL(NO_3)_2$ in order to understand the nature of intermolecular interactions in molecular packing observed in the solid state. Geometries optimizations of the complex were first carried out starting from the x-ray data. All computed values as well as experimental data are reported in table 8. Of all functionals used, HCTC in conjunction with SDD basis sets and the def2TZV fitting set seem to be the best in reproducing the experimental x-ray data. Pronounced differences were observed only for the LSDA functional, which provides a systematic shortening of all bond distances involving the metal atom. It was also observed a different behaviour towards the arrangement of the nitrobenzene terminal fragments that

in the solid state and in the geometries optimized with the functional CAM-B3LYP, HCTC and TPSSTPSS. They arrange themselves in such a way as to favor π-π interactions. This different arrangement is testified by the distances of C-C relative to the two pivot carbons carrying the nitro substituents and reported in table 8.

Table 8. Selected observed (RX), calculated bond distances (Å) around cadmium atoms and C…C separation (Å) for pivot carbons of nitrobenzene.

Functionals	Cd-N=	Cd-N-	Cd-O(NO_2)	C=N… N=C	CH_2NH …$NHCH_2$	$PhNO_2C$… ..CNO_2Ph
RX (Molecule 1)	2.3510	2.3701	2.3895	4.449	2.873	3.935
RX (Molecule 2)	2.3902	2.6552	2.5195	4.622	2.872	4.023
RX (Mean)	2.3706	2.5126	2.4545	4.536	2.8725	3.979
ITADUD[i]	2.3012	2.4381	-	7.767	2.986	-
QOHLOP[ii]	2.3050	2.355	-	4.507	2.887	-
VOQFOY[iii]	2.3030	2.3751	-	4.568	2.948	-
B3LYP/SDD	2.3453	2.3955	2.4055	4.4425	2.9131	8.9116
CAM-B3LYP/SDD	2.3251	2.3705	2.3705	4.3233	2.9195	3.7817
HCTC/SDD/def2TZV	2.3976	2.4404	2.3880	4.5109	2.9585	4.3157
HSEH1PBE/SDD	2.3157	2.3714	2.3891	4.3774	2.8890	8.6793
LSDA/SDD/def2TZV	2.2160	2.3151	2.3905	4.1301	2.8678	8.5656
MPW1PW91/SDD	2.3184	2.3701	2.3904	4.3786	2.8887	8.5702
PBEPBE/SDD/def2TZV	2.3231	2.3905	2.4385	4.3873	2.9241	8.6086
TPSSTPSS/SDD/def2TZV	2.3363	2.3787	2.3771	4.3560	2.9336	4.5508

Apart from the numerous hydrogen bonds(HBs), as shown in Fig. 8 three different types of chalcogen bonds(ChB) are observed which are fundamental in the construction of the crystalline packing. One of the three intermolecular ChBs involves the two nitro groups coordinated to cadmium

centers. This strong interaction is realized between the O10 oxygen atom bound to Cd (Cd-O10, 2.662Å) and N16 atom af the second molecule present in the asymmetric unit cell (O10…N16, 3.062 Å) while the angle N8-O10--N16 is 94.19°. A second very strong interaction is observed between the non-coordinated oxygen atom of the nitro group bound to Cd and the nitrogen atom of the nitrobenzene group (N1..O9, 2.827 Å), the angle N8-O9 ... N1 is 136.57° very close to the direction of the lone-pair of the oxygen atom donor of ChB.

The other two ChBs involve two nitro phenyl groups of two independent molecules (N..O, 3.031 Å and 3.034 Å). In all the ChB interactions, the N···O separation is less than the sum of van der Waals radii of elements (3.07 Å). In order to understand the extent of the interactions in determining the whole molecular packing, a series of DFT calculations based on the x-ray geometry involving the nitrobenzene groups, was also performed. Accordingly, the energy potential profile was computed by varying the N···O distance from 2.800 Å to 50 Å by using appropriate variable steps (0.1 Å near the minimum, and increasing the step far from the minimum) with assumption the energy found at 50 Å as our zero. An interaction energy of 2.36 kcal mol^{-1} (BSSE corrected) was calculated corresponding to a minimum at 3.350 Å, which is very close to the experimentally observed N···O separation of 3.0335 Å (see fig. 9).

Even considering this small difference (0.44 kcal) between equilibrium distance observed in the solid state and minimum reached with the theoretical calculation, we can conclude that the interaction is partly attractive in nature. Besides, slight difference is surely determined by the overall balance of all other interactions, some HOMOs and LUMO of two interacting groups are depicting in fig. 9.

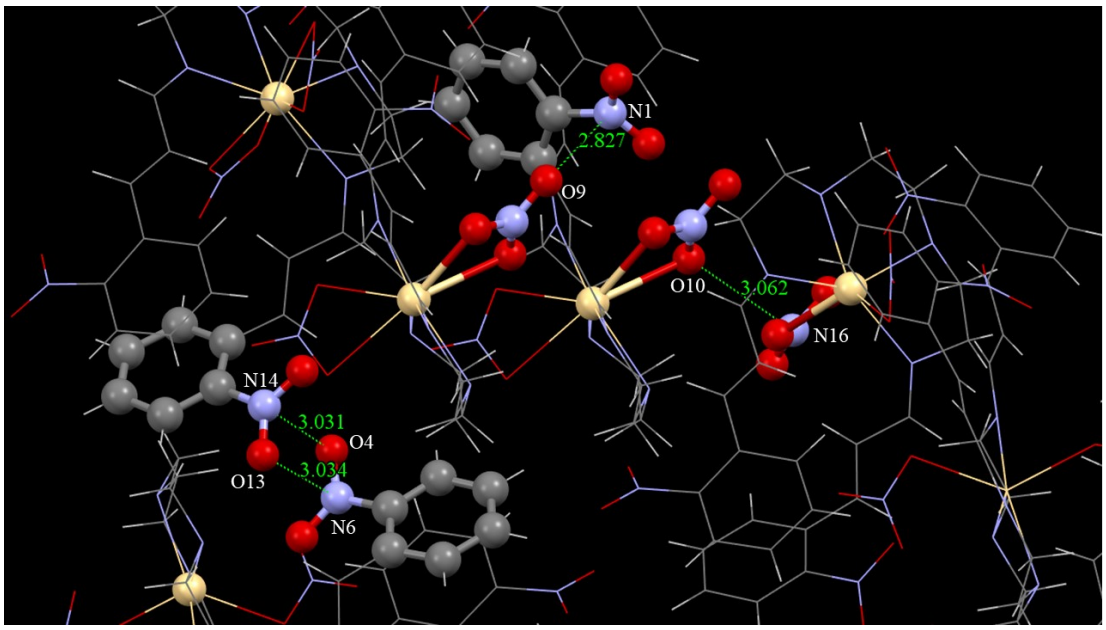

Fig.8. Three different Chalcogen bonds with the values of the O..N separations.

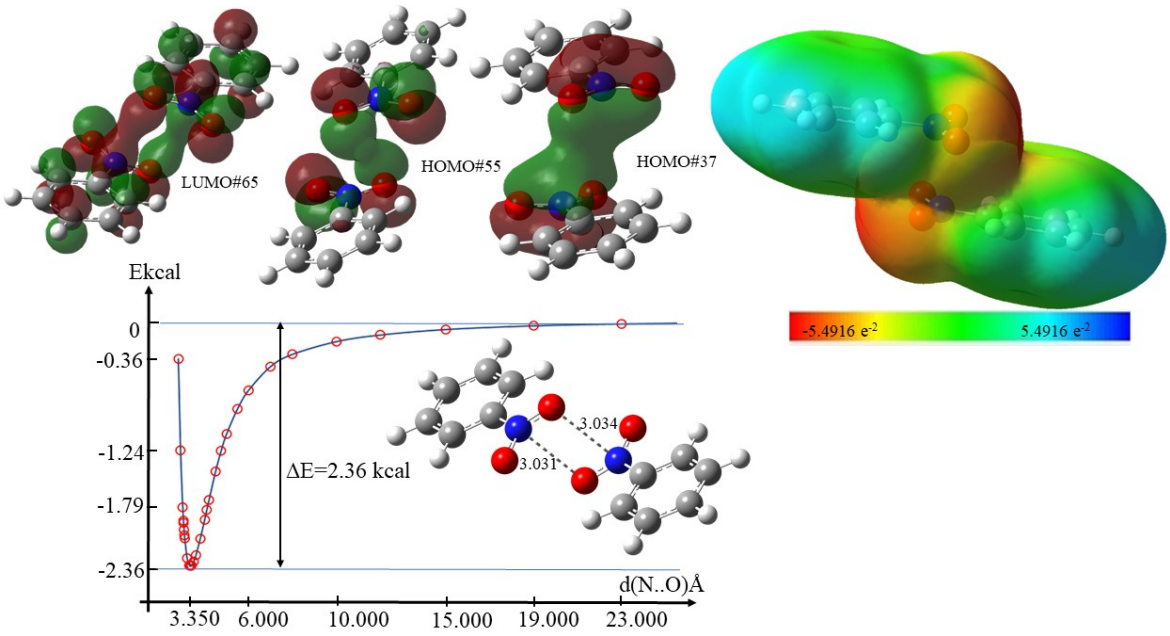

Fig.9. Molecular orbitals, electrostatic potentials and potential energy curve for the nitr-nitro interaction

3.6. Hirshfeld surface analysis of $CdL(NO_3)_2$ complex

Generally, to achieve the data related to non-covalent interactions, the fingerprint plots and Hirshfeld surfaces of the crystal packing of $CdL(NO_3)_2$ complex are utilized [48-52]. Accordingly herein, Hirshfeld surfaces of $CdL(NO_3)_2$ complex (Figs. 10, 11) were mapped over a d_{norm}, d_e, d_i as curvedness, fragment patch and shape-index.

The 2D fingerprint maps of $CdL(NO_3)_2$ complex gave several quantitative data concerning the probability of obtaining an extra understanding of intermolecular interactions in crystalline state as well as describing surface defining of molecules. Widely, H...O, H...H and H…C intermolecular interactions were found to be the most considerable in the crystal packing (49.5 %, 30.3 %, as well as 11.8 %). It is apparent that van

der Waals and hydrogen bond interactions induce a significant effect on the adjustment of the packing in the crystal framework, as well as another interconnects [N…O (1.8 %), N…H (1.7 %), C...C (1.6 %), O…C (0.7 %), C…O (0.7 %), C…N (0.2 %) and N…N (0.1 %)] that have less contribution with the Hirschfeld surfaces. The general obligation of various interactions to Hirshfeld surfaces was determined for $CdL(NO_3)_2$ complex as depicted in Figs. 12 and Fig.16S(SI).

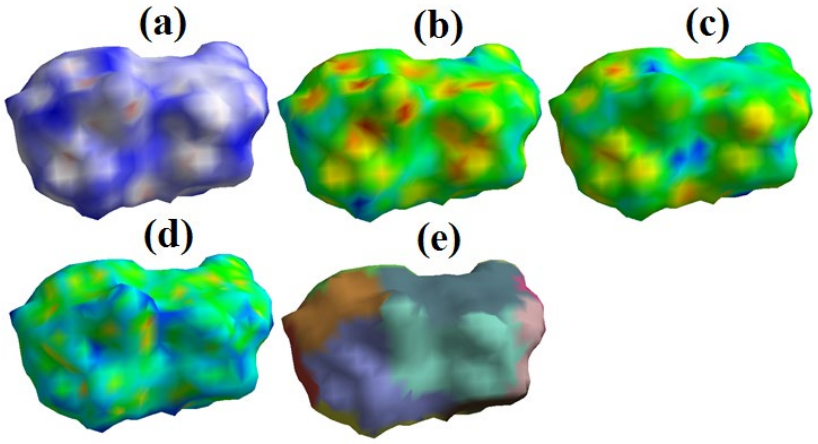

Fig 10. Hirshfeld surface analysis of $CdL(NO_3)_2$ complex: a) Normalized distance (d_{norm}); b) distance from a point on the Hirshfeld surface to the nearest external nucleus (d_e); c) distance from a point on the Hirshfeld surface to the closest internal nucleus (d_i); d) curvedness and e) fragment patch.

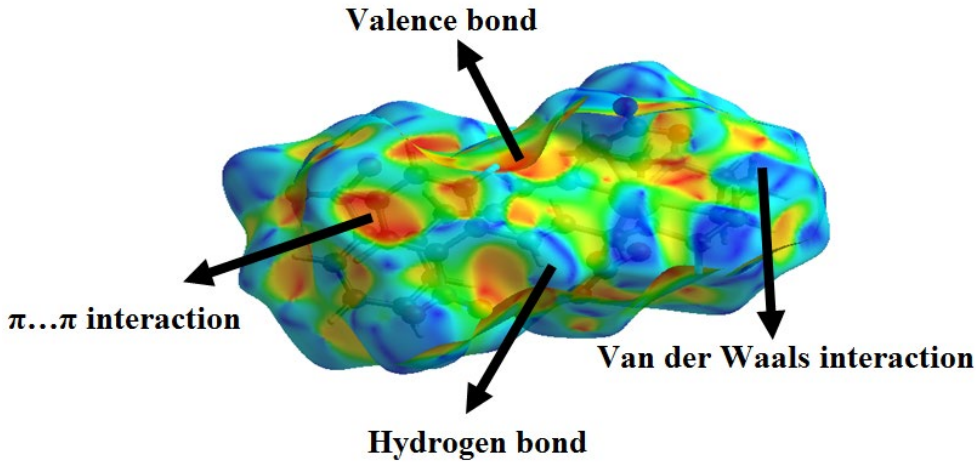

Fig 11. Hirshfeld surface of $CdL(NO_3)_2$ complex.

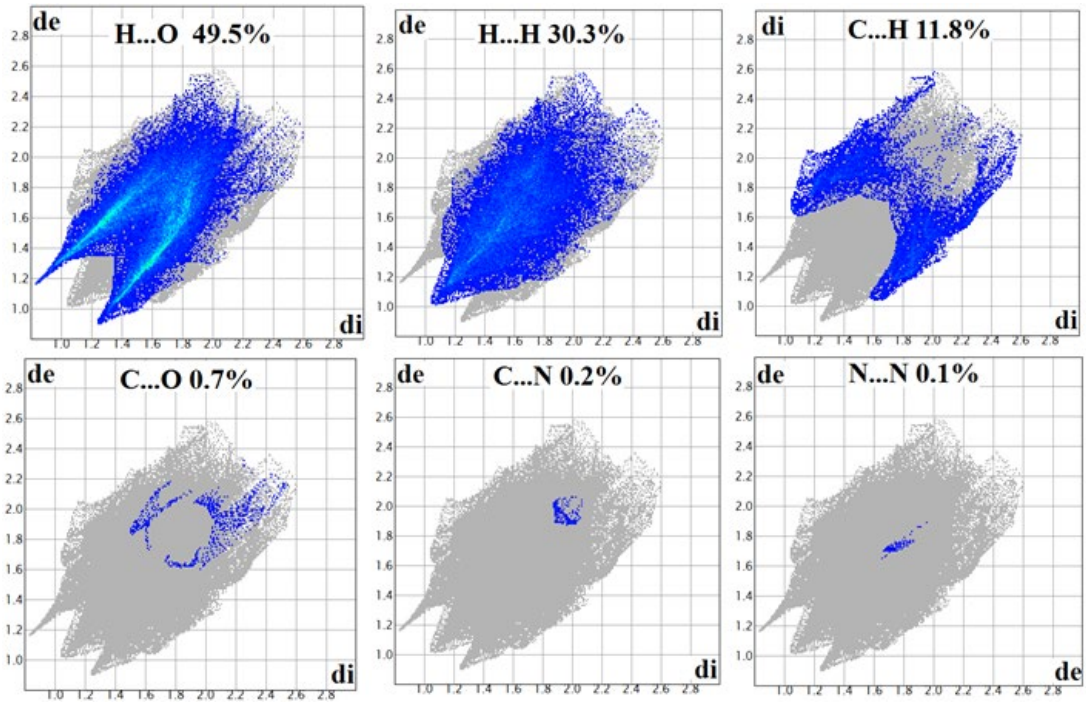

Fig 12. Fingerprint plots of major contacts in $CdL(NO_3)_2$ complex.

3.7. XRPD analysis

The synthesis of the compounds in ultrasonic bath results nanostructured complexes. Figs. of 13 and 14A shows the XRD pattern of cadmium(II) chloride, bromide and nitrate complexes prepared by the sonochemical process. The diffraction intensities were recorded from 10° to 80° (2θ angles). The considerable peaks in the patterns indicate that the particles have nanometer dimensions. Fig. 14 shows the comparison of two XRD patterns of the cadmium(II) nitrate complex, the one (A) related to the sonication-assisted prepared complex and the other (B) simulated from the single crystal X-ray data by MERCURY software [53]. The observed acceptable matches with slight differences in 2θ between two XRD patterns indicate a similar phase for this compound in both forms. The average size of the particles were estimated by the Scherer equation ($D = k\lambda/\beta Cos\theta$ where D is the average grain size, k is Blank's constant (0.891), λ is the X-ray wavelength (0.15405 nm), and θ and β are the diffraction angle and full width at half maximum of an observed peak, respectively [54]. According to XRD data analysis, the average particle size for $CdLCl_2$, $CdLBr_2$ and $CdL(NO_3)_2$ nanoparticles were found to be 11.49 nm, 25.20 and 11.62 nm, respectively.

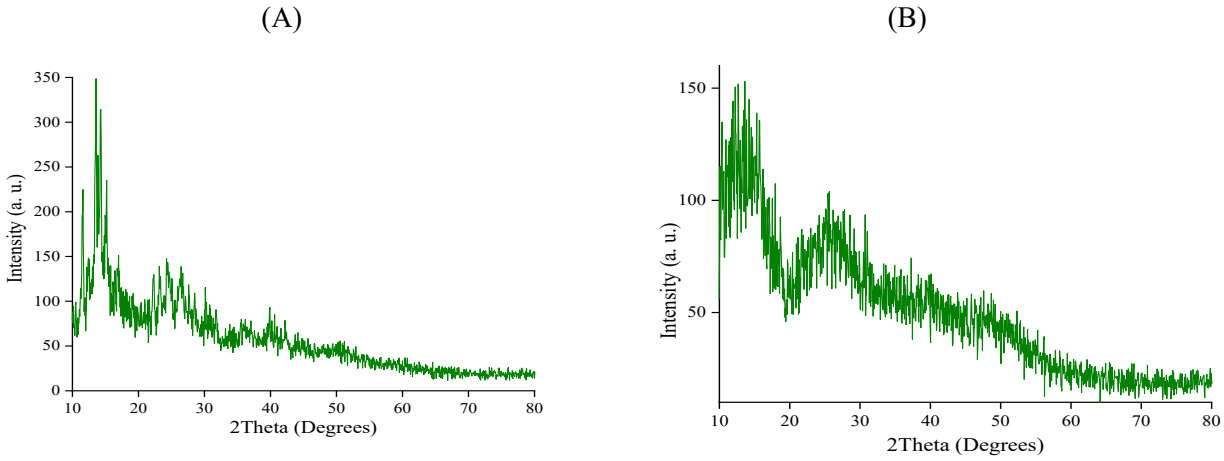

Fig. 13. XRD patterns of $CdLCl_2$ (A) and $CdLIBr_2$ (B)

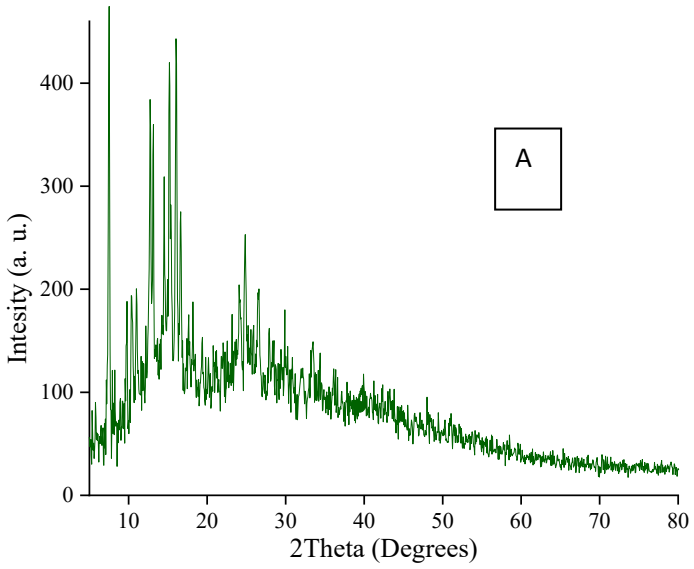

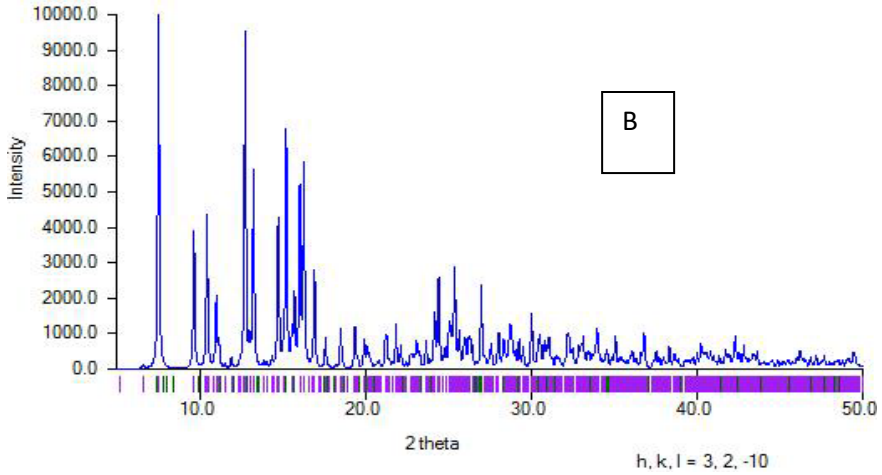

Fig. 14. The XRPD patterns of cadmium(II) nitrate complex nanoparticles (A) simulated from single crystal X-ray data (B)

3.8. SEM and EDAX of the compounds

SEM technique was applied to investigate the morphologies of ultrasound-assisted synthesized cadmium(II) compounds. The SEM images of $CdL(NO_3)_2$, $CdLCl_2$ and $CdLBr_2$ have been shown in Fig.15. Based on these pictures, the morphology of particles for cadmium(II) nitrate is observed as spherical in the solid state with the average size of about 20-30 nm in dimension while sheet and rod like shapes are observed for cadmium(II) chloride and cadmium(II) bromide respectively. Also, the distribution of particles in all four compounds is fairly uniform. As typical, the obtained EDAX plots of the cadmium(II) bromide and cadmium(II) nitrate complexes nanoparticles were recorded showing the presence of carbon, nitrogen and cadmium(II) as the elementary components (Fig.16)

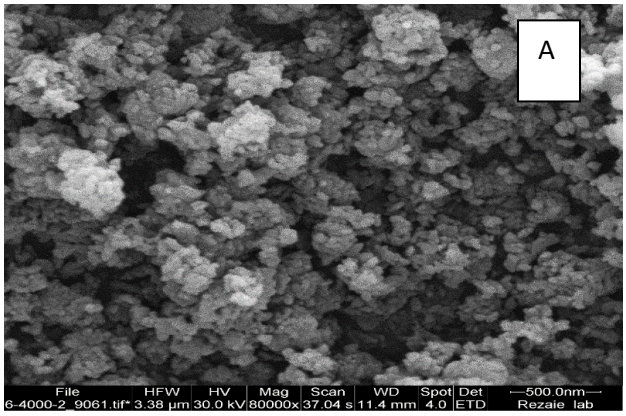

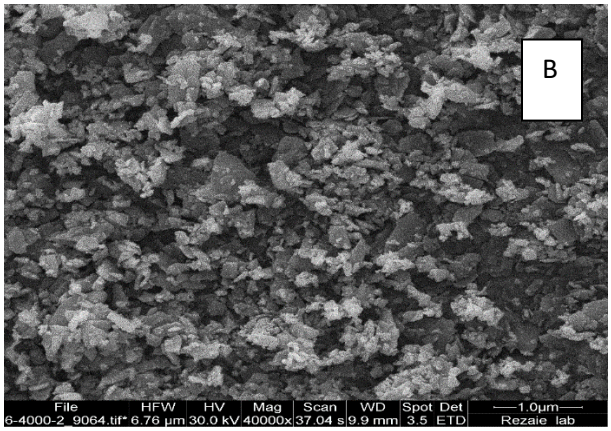

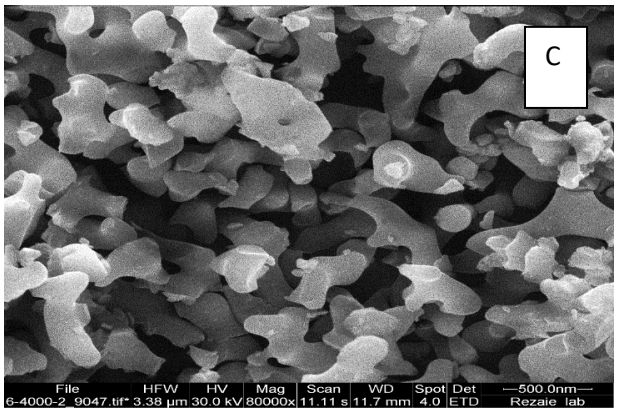

Fig. 15. The SEM images of (A) $CdL(NO_3)_2$, (B) $CdLCl_2$ and (C) $CdLBr_2$ complexes.

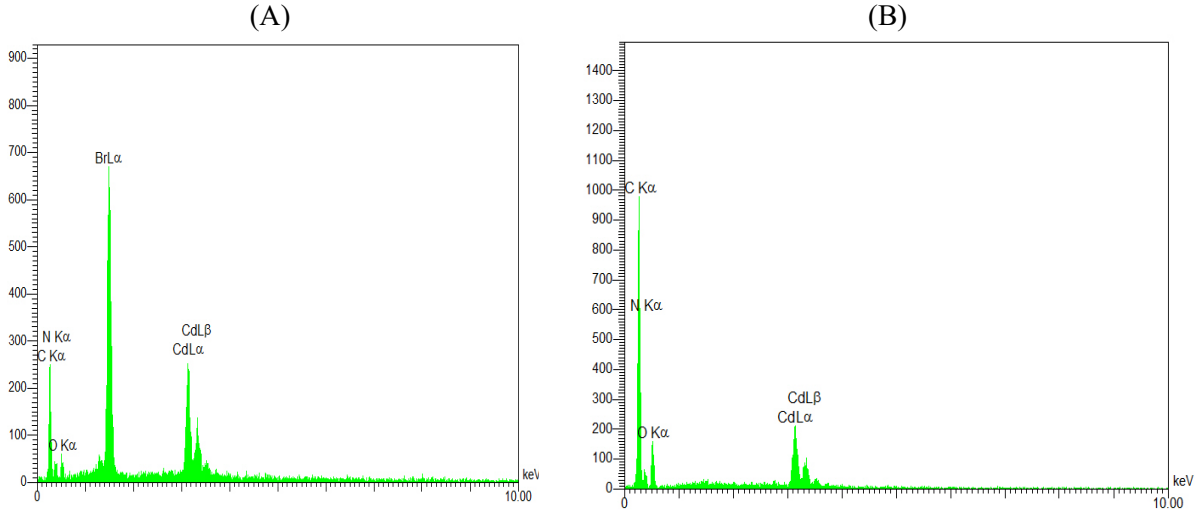

Fig. 16. EDAX analysis data of (A) $CdLBr_2$, (B) $CdL(NO_3)_2$ complex.

3.9. Characterization of cadmium(II) oxide nanoparticles

Nanoparticles of cadmium(II) oxide were prepared by direct thermolysis of cadmium(II) iodide complex at 600 ˚C for about 4 h and then were characterized by XRD and SEM (Fig. 17). Diffraction intensities recorded in 2θ angles from 5˚ to 50˚. The average size of 27.65 nm was evaluated for cadmium(II) oxide

nanoparticles by the Scherer equation. The SEM image of cadmium(II) oxide shows agglomerated and nonuniform spherical nanoparticles.

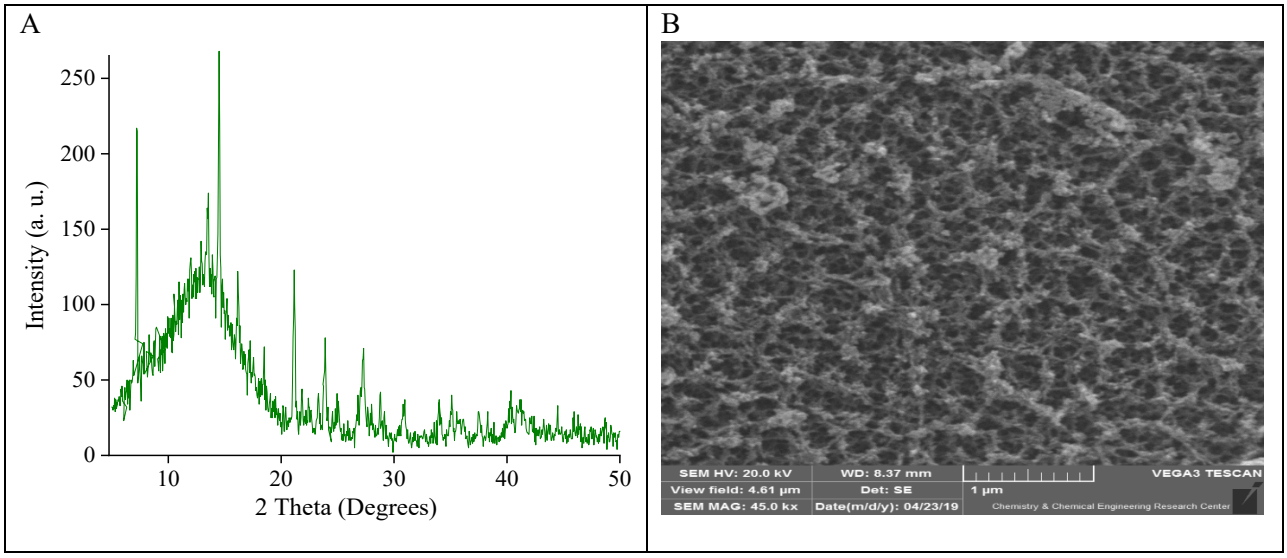

Fig. 17. The XRPD pattern (A) and SEM image (B) of cadmium(II) oxide nanoparticles.

3.10. Thermal investigation (TG/DTG/DTA)

The TG/DTG/DTA diagrams of the free ligand and its cadmium(II) complexes were carried out in the temperature range of 25-900 ˚C with the heating rates of 20 ˚C/min under N_2 atmosphere. As typical ones, TG/DTG/DTA of ligand, $CdLCl_2$ and $CdL(NCS)_2$ are presented in fig.18 and those for others are found as fig.12S in supplementary file. Indeed, the thermal analysis of the compound was carried out to obtain some information about the thermal stability of them. The thermal decomposition steps, mass loss (%), proposed lost segment, final residues and thermo-kinetic activation parameters of the ligand and its cadmium(II) complexes at each thermal decomposition step have been collected in tables of 9 and 10. The TGA diagram of the ligand shows its complete decomposition during one thermal step in the temperature range of 72-

580°C (Exp.= 95.77%, Calcd.=96.33%). According to TG/DTG/DTA thermal diagrams, $CdLCl_2$, $CdLI_2$ and $CdL(NCS)_2$ complexes are completely decomposed within 3 consecutive steps while the other complexes are decomposed as: $CdLBr_2$ within 4 thermal steps and, $CdL(NO_3)_2$ and $CdL(N_3)_2$ within 2 thermal steps. The proposed segments eliminated from the complexes have been suggested in tables 9. As a typical case, the proposed decomposition pathway for $CdLCl_2$ complex has been exhibited in Scheme 2. The cadmium(II) chloride complex loses about 34.25% (calcd. 33.15%) of its total mass at the first thermal step (107–276 °C). This mass reduction is attributed to elimination of $C_{10}H_2N_2O_4$ fragment. In the second thermal step (276–452 °C), complex loses about 7.29% (calcd. 10.92%) of its total mass, corresponding to elimination of $C_{12}H_{18}N_2$ part and in the third step (452-886 °C), decomposition process is accompanied by a mass reduction about 58.43% (Calcd. 55.46%) attributed to the removal of $C_2H_6Cl_2N_2Cd$ part. The residual mass at the end is trace amount of metallic cadmium. Furthermore, thermo-kinetic parameters such as activation energy (E^*), Arrhenius constant (A), enthalpy of activation (ΔH^*), entropy of activation (ΔS^*), and Gibbs free energy change (ΔG^*) of each decomposition step was calculated by employing the Coats–Redfern relation [55]. The obtained data have been collected in table 10. The activation energies of decomposition have been found in the range of 11.94-139.36 $kJ.mol^{-1}$ which these high values indicate thermal stability of the complexes. Positive value of the activation entropy ΔS^* (for example: at the first decomposition step of $CdLBr_2$ complex) reflects the dissociation nature of the process and the negative values of ΔS^* observed for other thermal steps of the complexes show more ordered activated complex than the reactants or a slower reaction rate than normal decomposition processes. [56]. In addition, the positive value of ΔG^* (1.18×10^2-3.01×10^2 KJ/mol) for the investigated compounds indicates that all thermal steps are nonspontaneous processes [57]. Finally, the positive values of ΔH^* (6.19 to 116.57KJ/mol) reflects the endothermic character of all thermal degradation steps.

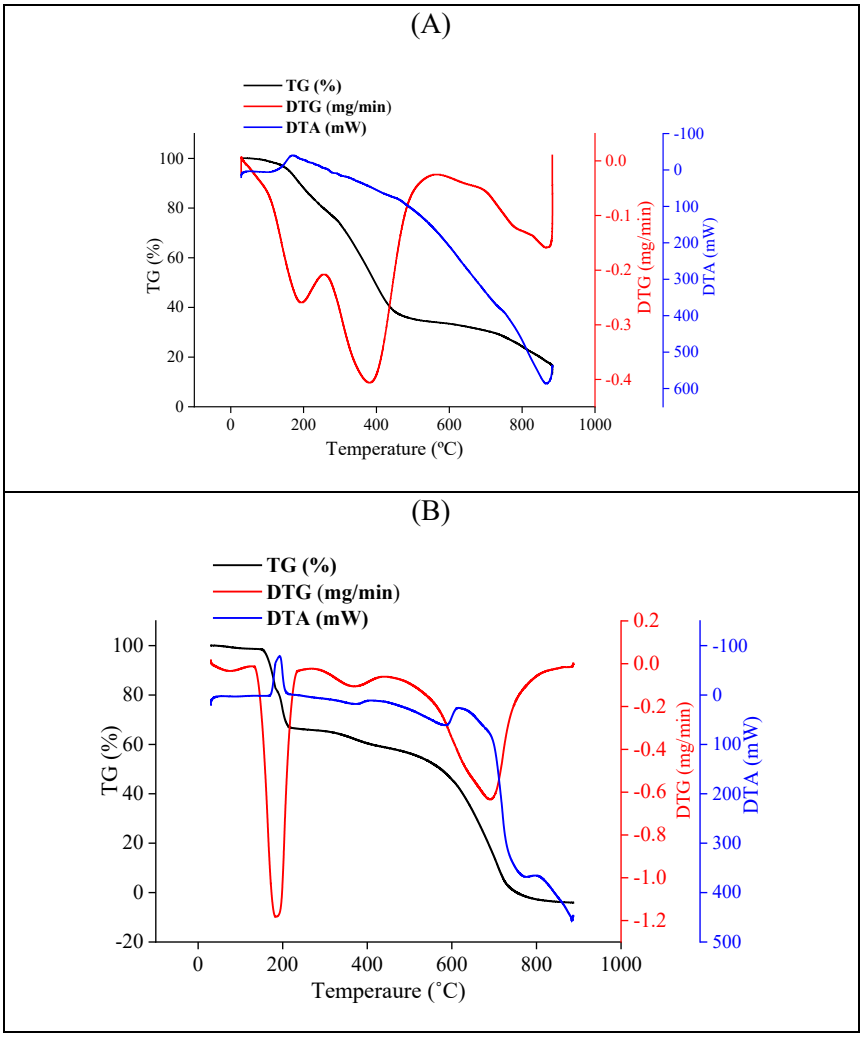

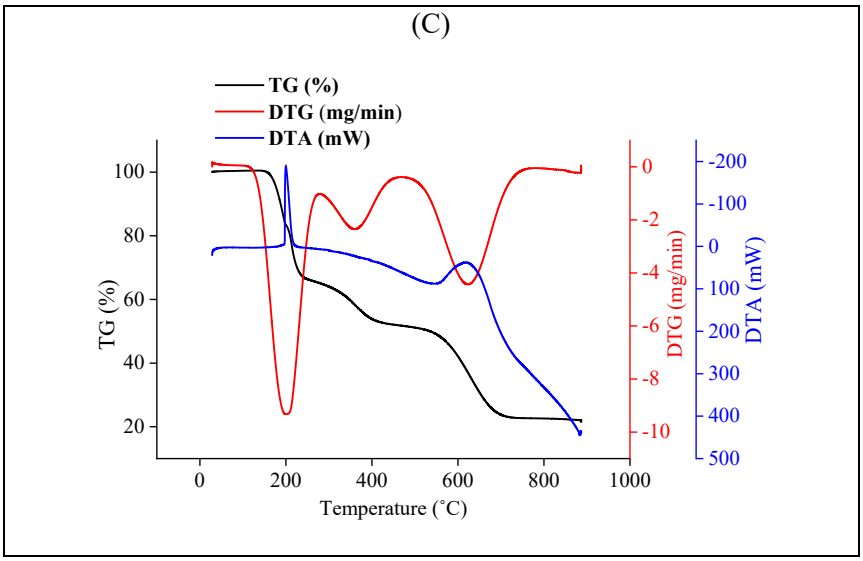

Fig. 18. TG/DTG/DTA curves of Schiff base ligand [A], $CdLCl_2$ [B], and $CdL(NCS)_2$ [C] complexes.

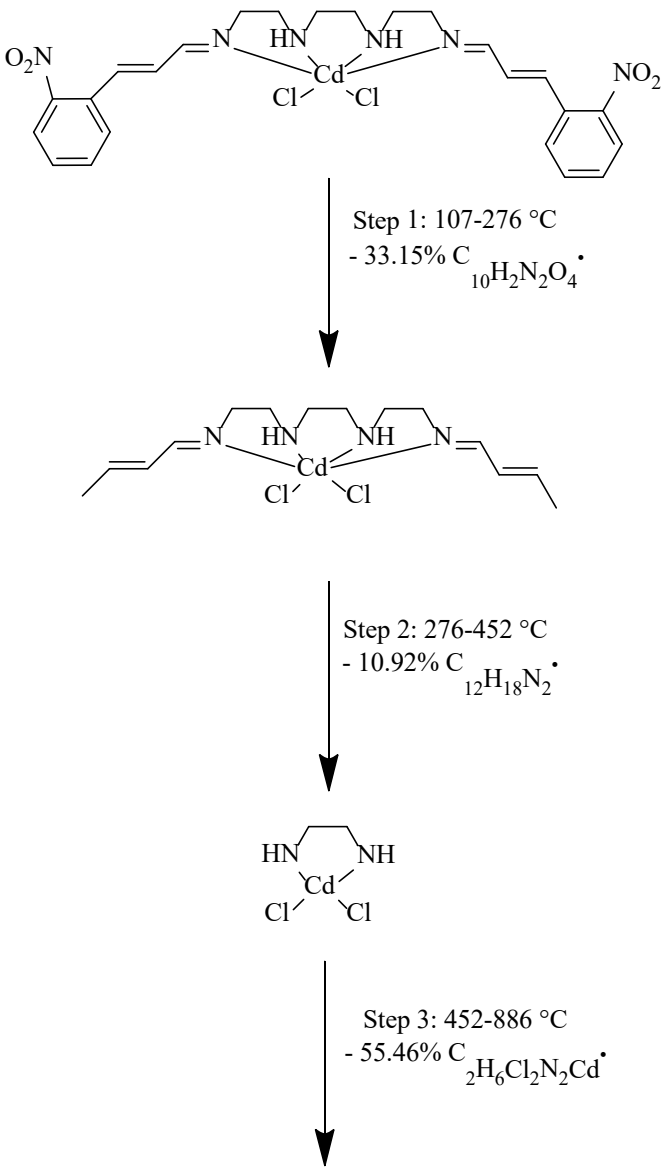

Scheme 2. The proposed decomposition pathway for $CdLCl_2$ complex

Table 9. Thermal analysis data of the Schiff base ligand and cadmium(II) complexes including temperature range, mass loss, differential thermal gravimetric (DTG) peak, proposed segment and final residuals.

Compound	Temperature range/ ˚C	Mass loss[found (Calculated)]/ %	DTG peak/ ˚C	Proposed segment	Final residue
Ligand	72-580	95.77 (96.33)	326.07	$C_{24}H_{28}N_6O_4$	-
$CdLCl_2$	107-276	34.25 (33.15)	191.86	$C_{10}H_2N_2O_4^{\bullet}$	Trace Cd
	276-452	7.29 (10.92)	364.49	$C_{12}H_{18}N_2^{\bullet}$	
	452-753	58.43 (55.46)	669.67	$C_2H_6Cl_2N_2Cd^{\bullet}$	
$CdLBr_2$	142-248	8.33 (6.12	212.44	NO_2	Trace Cd
	248-403	13.69 (16.36)	350.44	C_9HNO_2	
	403-577	27.12 (26.6)	550.26	$C_{15}H_{26}N_4$	
	577-763	50.86 (46.79)	660.78	$Br_2Cd_{0.9}$	
$CdLI_2$	100-263	20.47 (22.39)	182.1	$C_6H_2N_2$	$Cd_{0.5}$
	263-548	34.53(26.03)	521.87	$C_{18}H_{30}N_4$	
	548-749	42.99 (48.19)	655.27	$I_2Cd_{0.5}$	
$CdL(NO_3)_2$	144-282	77.83 (75.15)	214.68	$C_{24}H_{28}N_7O_7$	Trace Cd
	282-684	15.22 (18. 44)	513.64	$NO_3Cd_{0.9}$	
$CdL(NCS)_2$	121-265	34.30 (35.33)	193.34	$C_{12}H_8N_2O_4$	$Cd_{0.45}$
	265-448	13.57 (13.47)	365.94	$C_{12}H_{20}N_2$	
	448-777	29.48 (28.8)	612.92	$C_2N_2S_2Cd_{0.55}$	
$CdL(N_3)_2$	142-297	73.18 (76.63)	257.23	$C_{24}H_{28}N_9O_4$	Trace Cd
	297-613	18.19 (16.09)	430.8	$C_2H_6N_2Cd_{0.9}$	

Table 10. Thermokinetic activation parameters of the thermal decomposition steps of the Schiff base ligand and its cadmium(II) complexes

Compound	Decomposition step (˚C)	E^* (kJ mol^{-1})	A^* (s^{-1})	ΔS^* (kJ mol^{-1} K^{-1})	ΔH^* (kJ mol^{-1})	ΔG^* (kJ mol^{-1})
Ligand	72-580	139.36	5.72×10^{11}	-2.56×10^{1}	134.38	1.50×10^{2}
$CdLCl_2$	107-276	50.20	8.87×10^{2}	-1.92×10^{2}	46.33	1.36×10^{2}
	276-452	11.94	2.04×10^{-3}	-3.03×10^{2}	6.64	2.00×10^{2}
	452-753	60.21	3.25×10^{-1}	-2.64×10^{2}	52.37	3.01×10^{2}
$CdLBr_2$	142-248	130.20	8.03×10^{13}	1.72×10^{1}	126.16	1.18×10^{2}
	248-403	40.40	7.07×10^{-1}	-2.54×10^{2}	35.21	1.94×10^{2}
	403-577	93.82	2.27×10^{3}	-1.89×10^{2}	86.97	2.45×10^{2}
	577-763	95.92	2.43×10^{2}	-2.09×10^{2}	88.16	2.83×10^{2}
$CdLI_2$	100-263	15.89	3.48×10^{-3}	-2.96×10^{2}	12.10	1.47×10^{2}
	263-548	81.94	5.24×10^{2}	-2.01×10^{2}	78.33	2.35×10^{2}
	548-749	56.10	2.70×10^{-1}	-2.56×10^{2}	48.38	2.95×10^{2}
$CdL(NO_3)_2$	144-282	120.62	2.86×10^{12}	-1.06×10^{1}	116.57	1.22×10^{2}
	282-684	29.29	9.39×10^{-3}	-2.92×10^{2}	23.00	2.44×10^{2}
$CdL(NCS)_2$	121-265	101.28	1.91×10^{10}	-5.18×10^{1}	23.91	1.22×10^{2}

	265-448	22.80	1.04×10^{-2}	-2.89×10^{2}	51.56	2.00×10^{2}
	448-777	41.87	2.84×10^{2}	-2.84×10^{2}	34.50	2.86×10^{2}
$ZnCdL(N_3)_2$	142-297	74.98	7.89×10^{5}	-1.36×10^{2}	70.88	1.38×10^{2}
	297-613	12.10	4.38×10^{-3}	-2.97×10^{2}	6.19	2.17×10^{2}

3.11. *In-vitro* antimicrobial bioassay

The *in vitro* antibacterial activity of the free ligand and its cadmium(II) complexes were evaluated against two Gram-positive (*S. aureus* and *B. subtilis*) and two Gram-negative (*E. coli* and *P. aeruginosa*) bacteria by well diffusion method. The data of antibacterial activity are expressed as diameter of the inhibition zone of the growth (mm) against the above mentioned bacteria. The obtained data from experiments have been summarized in table 11. The resultant data for the ligand and its cadmium(II) complexes revealed that the complexation of the ligand increases the antibacterial activities. According to table 11, $CdLI_2$ complex is the most active compound and $CdL(NCS)_2$ complex is the lowest active compound against Gram-positive (*S. aureus* and *B. subtilis*). Other compounds showed similar activity against *S. aureus* and *B. subtilis*. $CdLBr_2$ was the most active compound against *E. coli* with an inhibition zone diameter of 23 mm whereas ligand shows the lowest activity. In the case of *P. aeruginosa*, the antibacterial activity can be ordered as $CdLI_2 > CdLBr_2 > CdL(NO_3)_2 \sim CdL(NCS)_2 > CdL(N_3)_2 > CdLCl_2 >$ Ligand. Also, the lowest activity against all bacteria is related to Schiff base ligand. Moreover a comparison of acquired results with some standard drugs including amoxicillin, penicillin and cephalexin [58] showed that the synthesized compounds have acceptable activities against all above mentioned bacteria.

In addition to the above investigation, the MIC and MBC data of all the compounds were also evaluated by the Mueller Hinton broth technique (Table 12). The MICs were found in the range of 39.06–625, 39.06–312.5, 39.06–625, and 39.06–312.5 μg/mL against for four types of bacteria of *B. subtilis, S. aureus, P. aeruginosa* and *E. coli,* respectively. It is to be noted that the compounds with low MIC and MBC

demonstrate better antibacterial activity. In the case of *B subtilis*, it was observed that $CdLI_2$ with MIC value of 39.06 µg /mL and MBC value of 78.12 µg /mL is the best inhibitor compound. Against the *S. aureus*, the ligand and $CdLCl_2$ complex with the same MIC values is the lowest effective compounds. Among the cadmium(II) complexes tested, $CdLI_2$ and $CdLCl_2$ with the same MIC value of 39.06 µg /mL showed the highest inhibitory effect against *P. aeruginosa*. In final, the growth of *E. coli* can be effectively stopped by $CdL(NO_3)_2$ with lower MIC value with respect to other compounds.

Table 11. Antibacterial activity of the ligand and its cadmium(II) complexes (12.5, 25 and 50 mg/mL) as diameter of zone of inhibition (mm).

	Gram positive bacteria						**Gram negative bacteria**					
	Bacillus subtilis			***Staphylococcus aureus***			***Pseudomonas aeruginosa***			***Escherichia coli***		
Compound (mg/mL)	12.5	25	50	12.5	25	50	12.5	25	50	12.5	25	50
L	10	13	12	9	11	20	4	5	5	8	10	10
$CdLCl_2$	14	16	20	12	16	22	6	8	8	13	14	15
$CdLBr_2$	14	15	23	19	20	22	6	11	19	21	23	23
$CdLI_2$	23	31	32	15	19	30	11	17	20	9	11	20
$CdL(NO_3)_2$	9	13	28	15	19	20	7	8	10	15	17	19
$CdL(NCS)_2$	10	11	11	13	18	18	7	8	10	10	11	11
$CdL(N_3)_2$	12	14	18	17	18	23	7	8	9	7	9	12
DMSO	-	-	-		-	-	-	-	-	-	-	-

Table 12. MIC and MBC data of Schiff base ligand and its cadmium(II) complexes in µg /mL for inhibition from the growth.

	Bacillus subtilis		***Staphylococcus aureus***		***Pseudomonas aeruginosa***		***Escherichia coli***	
Compound	MIC	MBC	MIC	MBC	MIC	MBC	MIC	MBC
Ligand	625	1250	312.5	625	625	1250	312.5	625
$CdLCl_2$	312.5	625	312.5	625	156.2	312.5	39.06	78.12
$CdLBr_2$	625	1250	156.2	312.5	39.06	78.12	39.06	78.12
$CdLI_2$	39.06	78.12	39.06	78.12	39.06	78.12	39.06	78.12
$CdL(NO_3)_2$	156.2	312.5	19.5	39.06	78.12	156.2	19.5	39.06
$CdL(NCS)_2$	312.5	625	156.2	312.5	78.12	156.2	156.2	312.5

$CdL(N_3)_2$	156.2	312.5	78.12	156.2	156.2	312.5	156.2	312.5

The free ligand and its cadmium(II) complexes were also screened against *C. albicans* and *A. niger* fungal strains. The bioassay experiments were performed using the well diffusion method and the results as the diameter of zone of inhibition (in mm) of the growth have been compiled in table 13. Similar to the previous section, the results showed that the Cd(II) complexes are more active with respect to their free Schiff base ligand under identical experimental conditions in all concentrations. In the case of *C. albicans*, among the complexes, $CdLCl_2$ and $CdL(NCS)_2$ showed the maximum and minimum activity, respectively. The general trend of the inhibition from growth against *C. albicans* is $CdLCl_2 > CdL(NO_3)_2 > CdLBr_2 > CdLI_2 > CdL(N_3)_2 > CdL(NCS)_2 > L$ and against *A. niger* is $CdLBr_2 > CdLCl_2 > CdL(NO_3)_2 \sim CdLI_2 > CdL(N_3)_2 > CdL(NCS)_2 > L$. In this work and many previous reports [59], increased biological activity of the coordination complexes with respect to the free ligand can be explained on the basis of Ross and Tweedy's chelation theory [60, 61]. It is suggested that the chelation reduces the polarity of the central metal because the positive charge of the metal ion is partially shared with the donor atoms of the Schiff base ligands and consequently π-electron delocalization over the whole chelate ring occurs [62]. The chelation could increase the lipophilic character of the metal atom that leads to easier transduction into the cell membrane. Thus, the metal ion of the complex can block the active site of the microorganisms enzyme causing the death of it [63].

Table 13. Antifungal activity of the ligand and its cadmium(II) complexes as diameter of zone of inhibition (mm).

	Candida albicans			*Aspergillus niger*		
Compound(mg /mL)	12.5	25	50	12.5	25	50
Ligand	4	4	5	4	5	5
$CdLCl_2$	23	23	24	22	24	29

$CdLBr_2$	-	18	19	26	31	32
$CdLI_2$	-	14	16	19	24	25
$CdL(NO_3)_2$	20	21	23	20	22	25
$CdL(NCS)_2$	-	9	10	6	7	18
$CdL(N_3)_2$	-	10	11	19	19	21

Generally, it is to be noted that various factors such as the nature of cell wall and structural properties of the compounds effect on potency of the compounds against bacteria and/or fungi. Both two factors can cause deformation/destruction of cell wall via passage of the compounds into cell or cleavage of bacteria or fungi DNA via intercalating or binding of the compound to it after diffusion into cell leading to microorganism death. Accordingly, it is really difficult to prove which reason is of more importance and only some suggestions for activity-structure relationship is possible. About more potency of cadmium iodide complex against bacteria may be due to more diffusion into cell wall because of its less polarity of this complex with respect to others leading to more destructive effect during its passage. On other hand, in these cases, after diffusion, cadmium iodide complex can also destruct the DNA bacteria via effective intercalation due to its steric hindrance. Each of these suggestions may be responsible for more inhibitory effect of this complex as compared with other ones. In antifungal screening, $CdLCl_2$ was mostly found more active than others. Herein, it is suggested that relatively more polar Cd-Cl bonds in cadmium chloride complex with respect to other Cd-X induces more positive charge ($+\delta$) on the cadmium center leading to more tendency to receive coordinative donor atoms of cell wall and enzymes or DNA structure after its diffusion into cell of treated fungi that this occurrence may be led to destruction of cell wall and/or stoppage of biochemical functions and therefore causes the death of microorganism. A part of above suggestions is also in agreement with DNA cleavage potency of compound as described in the next section.

3.12. DNA cleavage potential

Free Schiff base ligand and its cadmium(II) complexes were investigated for their interaction with extracted DNA of *E coli* by agarose gel electrophoresis method. Accordingly, the DNA cleavage activities of the compounds are depicted in Fig. 19. Lanes La, P, H and Li are lables for ladder, DNA (DNA alone) and the mixture of DNA and H_2O_2 and ligand, respectively. Lanes **A** to **F** refer to the mixture of DNA with $CdLCl_2$, $CdLBr_2$, $CdLI_2$, $CdL(NO_3)_2$, $CdL(NCS)_2$, and $CdL(N_3)_2$, respectively. If any compound behaves similar to

H_2O_2, it is suggested to be a cleaver agent while appearance of DNA band similar to lane P proposes the lock of cleavage potential for the compound. According to Fig. 19, it is perceived that complexes $CdLCl_2$, $CdLI_2$ and $CdL(NSC)_2$ cleave DNA completely while $CdL(N_3)_2$ and $CdLBr_2$ show moderate activity and $CdL(NO_3)_2$ has better than of these two complexes. Worth mentioning that, the Schiff base ligand has partial potential for the DNA cleavage as compared to its coordination compounds. The more activity of the cadmium(II) complexes may be due to efficient binding to DNA via coordination of its donor sites to metal center leading to degradation of DNA by them. The observed potency of the complexes for DNA cleavage may be a powerful reason for their antibacterial and antifungal activity after diffusion of the compound into micro-organisms cell besides other reasons such as cell wall destruction via effective binding or diffusion through it.

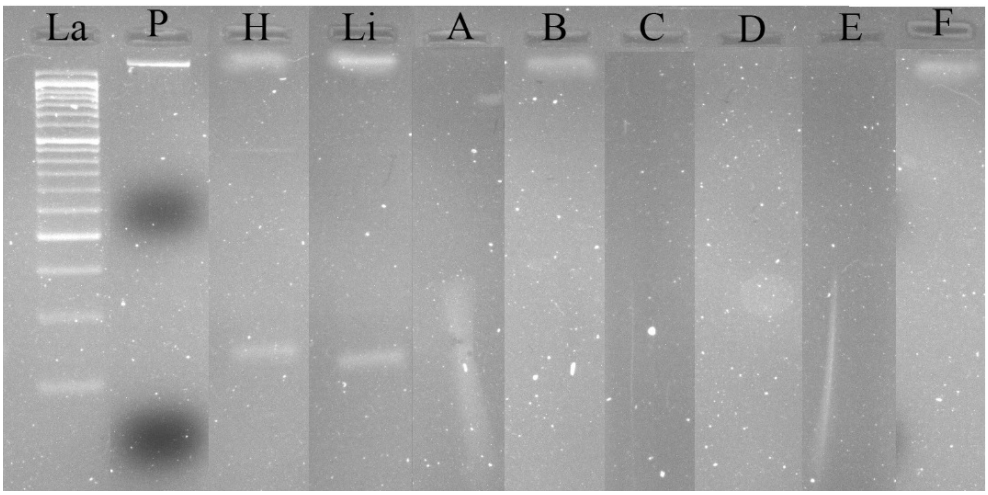

Fig. 19. Gel electrophoresis photograph for DNA cleavage activities of ligand and its cadmium(II) coordination compounds. Lanes of A to F: $CdLCl_2$, $CdLBr_2$, $CdLI_2$, $CdL(NO_3)_2$, $CdL(NCS)_2$ and $CdL(N_3)_2$ respectively, lane La: ladder, lane P: (DNA alone), lane H: (DNA+ H_2O_2) and lane Li: free ligand.

4. Conclusion

In this work, a new *N4*-tetradentate Schiff base ligand and its cadmium(II) halide/pseudo halide complexes were synthesized and characterized. Single crystal X-ray structure of cadmium(II) nitrate complex as typical showed molecular nature for the titled complexes. Accordingly $CdL(NO_3)_2$ complex crystallizes in monoclinic with space group of $P2_1/n$. Notable point in this structure analysis was observation of two coordination modes of nitrate groups and therefore two coordination number for Cd(II). Hirshfeld surface analysis showed that H...O, H...H and H…C intermolecular interactions were most considerable in the crystal packing. Moreover, the TG/DTGDTA analysis showed that the decomposition of ligand happens during one thermal step without any residue while the cadmium(II) complexes are thermally decomposed during 2-4 successive thermal steps leaving out metallic cadmium as final residue. Thermo-kinetic activation parameters well support thermal stability of the compound at room temperature. Furthermore, antimicrobial screening of the compounds showed that the complexes inhibit from the growth of the bacteria and fungi more efficient than free ligand. Moreover the results showed the complexes have more inhibitory effect against Gram-positive bacteria as compare with Gram-negative candidates. The cadmium complexes, especially cadmium halide complexes were found more active against *Aspergillus niger* with respect to *Candida albicans.* The DNA cleavage studies (by agarose gel electrophoresis method) confirmed that most of the complexes can efficiently degrade DNA Finally, the direct calcination of cadmium(II) iodide complex showed this type of complexes can be used as precursor compound for preparation of cadmium(II) oxide nanoparticles.

Acknowledgements

Partial support of this work by Yasouj University is appreciated.

Data Availability Statement

The data that support the findings of this study are available from the corresponding author upon reasonable request.

Supporting Information

Crystallographic data for this paper with CCDC number of 2015485 are available free of charge at http://www.ccdc.cam.ac.uk/conts/retrieving.html. All ^{1}H and ^{13}C NMR spectra, TG/DTG/DTA and some other figures supporting the results are found in supplementary file of this paper.

References

[1] J.-W. Cui, S.-X. Hou, K. Van Hecke, G.-H. Cui, *Dalton Trans.* **2017**, 46, 2892-2903.
[2] S.Y. Hao, S.X. Hou, K. Van Hecke, G.H. Cui, *Dalton Trans.* **2017**, 46, 1951-1964.
[3] M. Montazerozohori, S.M. Jahromi, A. Naghiha, *Ind. Eng. Chem* **2015**, 22, 248-257.
[4] K. Aoki, I. Fujisawa, K. Murayama, N.-H. Hu, *Coord. Chem. Rev* **2013**, 257, 2798-2813.
[5] V.P. Brahmkhatri, K. Chandra, A. Dubey, H.S. Atreya, *Nanoscale* **2015**, 7, 12921-12931.
[6] M. Shebl, S.M. Khalil, S.A. Ahmed, H.A. Medien, *J. Mol. Struct* **2010**, 980, 39-50.
[7] G. Kumar, V. Singh, K. Singh, I. Ahmad, D.S. Yadav, A. Kumar, N. Shishodia, *J. Pharm.* **2012**, 2, 45-49.
[8] C.L. Cahill, D.T. de Lill, M. Frisch, *CrystEngComm* **2007**, 9, 15-26.
[9] A. Morsali, L.G. Zhu, *Helv. Chim. Acta* **2006**, 89, 81-93.
[10] Y. Hasegawa, T. Nakanishi, *RSC Adv* **2015**, 5, 338-353.
[11] J.-N. Rebilly, B. Colasson, O. Bistri, D. Over, O. Reinaud, *Chem. Soc. Rev* **2015**, 44, 467-489.
[12] P. Zanello, *Coord. Chem. Rev* **2014**, 280, 54-83.
[13] V. Safarifard, A. Morsali, *Ultrason Sonochem* **2012**, 19, 300-306.
[14] V. Safarifard, A. Morsali, *Ultrason Sonochem* **2014**, 21, 253-261.
[15] R. Moosavi, A.R. Abbasi, M. Yousefi, A. Ramazani, A. Morsali, *Ultrason Sonochem* **2012**, 19, 1221-1226.
[16] A.R. Abbasi, H. Kalantary, M. Yousefi, A. Ramazani, A. Morsali, *Ultrason Sonochem* **2012**, 19, 853-857.
[17] R. Arabian, A. Ramazani, B. Mohtat, V. Azizkhani, S.W. Joo, M. Rouhani, *J. Energetic Mater* **2014**, 32, 300-305.
[18] J.H. Bang, K.S. Suslick, *Adv. Mater* **2010**, 22, 1039-1059.

[19] P.G. Derakhshandeh, J. Soleimannejad, J. Janczak, *Ultrason Sonochem* **2015**, 26, 273-280.
[20] P. Sun, S. Liu, J. Han, Y. Shen, H. Sun, D. Jia, *Transition Met. Chem.* **2017**, 42, 387-393.
[21] S. Kumar, R.P. Sharma, P. Venugopalan, V.S. Gondil, S. Chhibber, T. Aree, M. Witwicki, V. Ferretti, *Inorg. Chim. Acta* **2018**, 469, 288-297.
[22] R. Jayakrishnan, G. Hodes, *Thin Solid Films* **2003**, 440, 19-25.
[23] M. Ristić, S. Popović, S. Musić, *Mater. Lett.* **2004**, 58, 2494-2499.
[24] M. Montazerozohori, S. Yadegari, A. Naghiha, S. Veyseh, *Ind. Eng. Chem* **2014**, 20, 118-126.
[25] M. Montazerozohori, S. Zahedi, A. Naghiha, M.M. Zohour, *Mater. Sci. Eng* **2014**, 35, 195-204.
[26] M. Montazerozohori, A. Nazaripour, A. Masoudiasl, R. Naghiha, M. Dusek, M. Kucerakova, *Mater. Sci. Eng* **2015**, 55, 462-470.
[27] M. Montazerozohori, S. Musavi, A. Masoudiasl, A. Hojjati, A. Assoud, *Spectrochim. Acta A* **2015**, 147, 139-150.
[28] M. Montazerozohori, S.M. Jahromi, A. Masoudiasl, P. McArdle, *Spectrochim. Acta A* **2015**, 138, 517-528.
[29] M. Montazerozohori, S.A. Musavi, *J Coord Chem* **2008**, 61, 3934-3942.
[30] M. Montazerozohori, S. Farokhiyani, A. Masoudiasl, J. White, *RSC Adv* **2016**, 6, 23866-23878.
[31] M. Montazerozohori, A. Masoudiasl, T. Doert, *Inorg. Chim. Acta* **2016**, 443, 207-217.
[32] S.G. Niyaky, M. Montazerozohori, A. Masoudiasl, J. White, *J. Mol. Struct* **2017**, 1131, 201-211.
[33] M. Frisch, G. Trucks, H.B. Schlegel, G.E. Scuseria, M.A. Robb, J.R. Cheeseman, G. Scalmani, V. Barone, B. Mennucci, G. Petersson, Gaussian 09, revision D. 01, Gaussian, Inc., Wallingford CT, 2009.
[34] R.H. Hertwig, W. Koch, *Chem. Phys. Lett.* **1997**, 268, 345-351.
[35] D. Andrae, U. Haeussermann, M. Dolg, H. Stoll, H. Preuss, *Theor. Chim. Acta* **1990**, 77, 123-141.
[36] J. Heyd, G.E. Scuseria, M. Ernzerhof, *J. Chem. Phys.* **2003**, 118, 8207-8215.
[37] J.P. Perdew, K. Burke, M. Ernzerhof, *Phys. Rev. Lett* **1996**, 77, 3865.
[38] F.A. Hamprecht, A.J. Cohen, D.J. Tozer, N.C. Handy, *J. Chem. Phys.* **1998**, 109, 6264-6271.
[39] J. Tao, J.P. Perdew, V.N. Staroverov, G.E. Scuseria, *Phys. Rev. Lett* **2003**, 91, 146401.
[40] C. Adamo, V. Barone, *J. Chem. Phys.* **1998**, 108, 664-675.
[41] A.D. Becke, *J. Chem. Phys.* **1992**, 96, 2155-2160.
[42] A. Masoudiasl, M. Montazerozohori, R. Naghiha, A. Assoud, P. McArdle, M.S. Shalamzari, *Mater. Sci. Eng* **2016**, 61, 809-823.
[43] I. Ali, W. A. Wani, K. Saleem, *Synth. react. Met.-Org. Nano-Met. Chem.* **2013**, 43, 1162-1170.
[44] F. K. Ommenya, E. A. Nyawade, M. Andala, J. Kinyua, *J. Chem.* **2020**, 1745236, 1-8.
[45] R.S.Bhaskar, C.A.Ladole, N.G.Salunkhe, J.M.Barabde, A.S.Aswar, *Arabian J. Chem.* **2020**, 13, 6559-6567.
[46] S. Mousavi, M. Montazerozohori, A. Masoudiasl, G. Mahmoudi, J. White, *Ultrason Sonochem* **2018**, 46, 26-35.
[47] J. Prywer, *Journal of crystal growth* **2004**, 270, 699-710.
[48] M.A. Spackman, D. Jayatilaka, *CrystEngComm* **2009**, 11, 19-32.
[49] O. Urgut, I. Ozturk, C. Banti, N. Kourkoumelis, M. Manoli, A. Tasiopoulos, S. Hadjikakou, *Inorg. Chim. Acta* **2016**, 443, 141-150.
[50] E. Bouaziz, C.B. Hassen, N. Chniba-Boudjada, A. Daoud, T. Mhiri, M. Boujelbene, *J. Mol. Struct* **2017**, 1145, 121-131.

[51] R.S. Bitzer, L.C. Visentin, M. Hörner, M.A. Nascimento, C.A. Filgueiras, *J. Mol. Struct* **2017**, 1130, 165-173.
[52] O. Urgut, I. Ozturk, C.N. Banti, N. Kourkoumelis, M. Manoli, A.J. Tasiopoulos, S.K. Hadjikakou, *Mater. Sci. Eng* **2016**, 58, 396-408.
[53] C.F. Macrae, P.R. Edgington, P. McCabe, E. Pidcock, G.P. Shields, R. Taylor, M. Towler, J. Streek, *J. Appl.Crystallogr* **2006**, 39, 453-457.
[54] J. Yang, C. Lin, Z. Wang, J. Lin, *Inorg. Chem* **2006**, 45, 8973-8979.
[55] A.W. Coats, J. Redfern, *Nature* **1964**, 201, 68-69.
[56] G. Consiglio, I.P. Oliveri, S. Failla, S. Di Bella, *Inorganics* **2018**, 6, 8.
[57] P. Maravalli, T. Goudar, *Thermochim. Acta* **1999**, 325, 35-41.
[58] M.A. Goher, F.A. Mautner, B. Sodin, B. Bitschnau, *J. Mol. Struct* **2008**, 879, 96-101.
[59] A. Jayamani, V. Thamilarasan, N. Sengottuvelan, P. Manisankar, S.K. Kang, Y.-I. Kim, V. Ganesan, *Spectrochim. Acta A* **2014**, 122, 365-374.
[60] G. Engelhardt, P. Wallnöfer, *Appl. Environ. Microbiol.* **1975**, 29, 717-721.
[61] B. Tweedy, *Phytopathology* **1964**, 55, 910-914.
[62] A.A. El-Sherif, M.M. Shoukry, M.M. Abd-Elgawad, *Spectrochim. Acta A* **2012**, 98, 307-321.
[63] M. Khorasani-Motlagh, M. Noroozifar, A. Akbari, S. Mirkazehi-Rigi, *J. Mol. Struct* **2015**, 1083, 57-64.